

## Two-Relaxation-Time Lattice Boltzmann Scheme: About Parametrization, Velocity, Pressure and Mixed Boundary Conditions

Irina Ginzburg<sup>1,\*</sup>, Frederik Verhaeghe<sup>2</sup> and Dominique d'Humières<sup>3</sup>

<sup>1</sup> *Cemagref, Antony Regional Centre, Parc de Tourvoie - BP 44, 92163 Antony Cedex, France.*

<sup>2</sup> *Department of Metallurgy and Materials Engineering, Katholieke Universiteit Leuven, Kasteelpark Arenberg 44, 3001, Leuven, Belgium.*

<sup>3</sup> *Laboratoire de Physique Statistique, École Normale Supérieure, associated to CNRS and P. and M. Curie and D. Diderot Universities, 24 Rue Lhomond, 75231 Paris Cédex 05, France.*

Received 14 Mar 2007; Accepted (in revised version) 22 July 2007

Communicated by Shiyi Chen

Available online 9 October 2007

---

**Abstract.** We develop a two-relaxation-time (TRT) Lattice Boltzmann model for hydrodynamic equations with variable source terms based on equivalent equilibrium functions. A special parametrization of the free relaxation parameter is derived. It controls, in addition to the non-dimensional hydrodynamic numbers, any TRT macroscopic steady solution and governs the spatial discretization of transient flows. In this framework, the multi-reflection approach [16, 18] is generalized and extended for Dirichlet velocity, pressure and mixed (pressure/tangential velocity) boundary conditions. We propose second and third-order accurate boundary schemes and adapt them for corners. The boundary schemes are analyzed for exactness of the parametrization, uniqueness of their steady solutions, support of staggered invariants and for the effective accuracy in case of time dependent boundary conditions and transient flow. When the boundary scheme obeys the parametrization properly, the derived permeability values become independent of the selected viscosity for any porous structure and can be computed efficiently. The linear interpolations [5, 46] are improved with respect to this property.

**PACS:** 47.10.ad, 47.56+r, 02.60-x

**Key words:** Lattice Boltzmann equation, Dirichlet boundary conditions, Chapman-Enskog expansion, multiple-relaxation-time model, BGK model, TRT model, Navier-Stokes equation, Stokes equation, recurrence equations, staggered invariants.

---

\*Corresponding author. *Email addresses:* [irina.ginzburg@cemagref.fr](mailto:irina.ginzburg@cemagref.fr) (I. Ginzburg), [frederik.verhaeghe@mtm.kuleuven.be](mailto:frederik.verhaeghe@mtm.kuleuven.be) (F. Verhaeghe), [dominiq@lps.ens.fr](mailto:dominiq@lps.ens.fr) (D. d'Humières)

## 1 Introduction

The two-relaxation-time (TRT) Lattice Boltzmann model [17–20] is suitable to model solutions of the Navier-Stokes and hyperbolic non-linear advective-diffusion equations. A very simple linear collision TRT operator is based on the decomposition of the population solution into its symmetric and anti-symmetric components. Two locally prescribed eigenvalues (relaxation parameters) determine the evolution of the symmetric and anti-symmetric collision components. When the eigenvalues are equal, the TRT reduces to the BGK operator [41] (called sometimes *single-relaxation-time*, SRT). The SRT and TRT solutions can be obtained using the multiple-relaxation-times (MRT) collision operator [15, 27–31, 36]. At second order, the incompressible macroscopic mass and momentum conservation equations are identical for TRT, SRT and MRT but these models differ for higher-order approximations.

For TRT and SRT, both the kinematic and bulk viscosity are related to the selected “symmetric” eigenvalue and the coefficients of the diffusion tensor are related to the prescribed “anti-symmetric” eigenvalue. The effective values of the transport coefficients depend also on the distribution of the equilibrium components between the different velocities: the hydrodynamic equations are usually modeled with isotropic equilibrium weights [41] whereas the anisotropic diffusion tensors need anisotropic ones (see [17, 19]). The TRT model enables a very simple analysis of its solutions based on parity arguments. One example presents the multi-reflection (MR) boundary schemes, first developed in [16] for the Navier-Stokes equation and then adapted in [18] for the symmetric equilibrium components, e.g., any scalar diffusion variable. Another example presents the analysis of the interface conditions in [20], suitable for flat interface between two immiscible fluids and for modeling Darcy flows in heterogeneous stratified soils.

There are strong numerical evidences (see [16]) that the permeability of an arbitrary porous media is independent of the chosen viscosity value when a specific combination of symmetric/anti-symmetric eigenvalues (so-called “magic parameter”, here  $\Lambda_{eo}$ ) is fixed and no-slip conditions are modeled either with the bounce-back or with one particular multi-reflection (MR1) scheme [16]. In other words, the obtained momentum distribution for Stokes flow, multiplied with the modeled viscosity, depends on the selected eigenvalues only via their combination  $\Lambda_{eo}$ . This property implies a very specific functional dependency of the coefficients on the eigenvalues for all the terms in the population expansion and boundary rules. The earlier exact solution [13] confirmed this for parabolic flow. In this paper we give a rigorous explanation of these observations for arbitrary flow, owing to the derivation in [32] of *equivalent* link-wise recurrence equations. They allow to demonstrate that any steady non-dimensional velocity and pressure TRT solution, obtained with the Stokes or Navier-Stokes equilibrium functions, is governed by  $\Lambda_{eo}$  on a given grid, in addition to the Reynolds, Froude and Mach numbers. We will show that bounce-back and MR1 share this property exactly.

In contrast with the SRT, the TRT can keep  $\Lambda_{eo}$  at any prescribed value for both hydrodynamic and convective-diffusion equations when their transport coefficients vary. This

property is especially important when the kinematic viscosity takes large values, e.g., for two phase flow with high viscosity ratio (see [20]), non-Newtonian fluids or simply for accelerating the convergence to steady state [16, 40]. The SRT model will result in high bulk and boundary discretization errors, related roughly to the square of viscosity coefficient. In contrast, the TRT model with a proper choice of its free relaxation parameter can reduce, at least, the spatial errors, and avoid a redundant variation of the characteristic parameters and collision eigenvalues. Besides that, the particular value  $\Lambda_{eo} = 1/4$  has remarkable properties for stability of mass-conservation equation (see [21]).

The multi-reflection boundary approach follows the principal idea of the early works [12, 14, 15, 44]. They look for the incoming population in the form of its expansion and insert the prescribed macroscopic boundary condition. Motivated by an exact modeling of the parabolic distributions (e.g., Poiseuille flow in inclined channels), the boundary techniques [12, 14, 16] are all based on a *third-order* expansion, but they differ for the approximation of the unknown gradients: finite-differences are used in [12], local equations are established in [14], appropriate linear link-wise combinations of the known populations are found in [16]. The MR conditions are much simpler than the node based schemes, e.g., in [12, 14, 33, 39, 44], or the diffusive “kinetic” schemes [3, 4, 43, 45], and can prescribe more easily distinct conditions on adjacent walls, e.g., in corners. Modeling the Stokes equation in porous media [16, 40] clearly demonstrated the superiority of the MR1 over linear/quadratic interpolations [5], both in accuracy and convergence. The MR1 scheme is extended to MGMR(C) family with exact parametrization and advanced stability properties. Modeling the solutions of the incompressible Navier-Stokes equation [16, 33] confirmed the accuracy of MR1 for velocity and pressure solutions with static and moving boundaries, but also revealed some difficulties with its applications in corners, a problem we address in this paper.

We formulate the linear interpolations presented in [5] but also those from [46] as a particular MR schemes and show that there is an infinite number of three population schemes of formally equivalent accuracy (LI-family below). Linear schemes do not maintain automatically the parametrization properties of the bulk solutions and their permeability values depend on the used viscosity value, as shown in [16, 40] for the linear schemes of [5]. One exception is presented in this paper (CLI scheme). We improve the deficiency of the linear interpolations with the help of a simple local link-wise correction (MGLI sub-family) and present third-order accurate two-point schemes (MLI family) which are exactly parameterized, then extend them for corners.

Known pressure boundary conditions are mostly restricted to solid walls located at grid nodes, either by prescribing the equilibrium distribution for the incoming population or by deriving their solution from a local system of mass/momentum constraints, e.g., in [49]. So far a simple link-wise approach is the first-order accurate *anti-bounce-back* rule. It defines the solution for the incoming populations on a free interface in [34] or for the diffusion equation in [18]. The pressure schemes developed in this paper localize the Dirichlet values at any prescribed distance along the link. The principal difference from the boundary schemes [18] for the advection-diffusion equations is in the treatment of

the first and second velocity gradients: we present second- and third-order accurate MR pressure schemes with exact parametrization properties.

A Dirichlet pressure condition is not sufficient to set the solution of the Navier-Stokes equations uniquely. As an example, we extend the MR approach to a mixed condition which prescribes the pressure and the tangential velocity. This scheme is a linear combination of the velocity and pressure multi-reflections, involving a whole set of cut links into the local combination. The mixed scheme is formulated for any shape of the wall, but we work out the details only for orientations of the boundary parallel to one of the main axes, using  $d2Q9$ ,  $d3Q15$  and  $d3Q19$  velocity sets as examples.

This paper is focused on the derivation and analysis of MR boundary schemes. A complementary part [22] validates them for steady and time-harmonic flows with exact solutions. Section 2 develops the TRT hydrodynamic model. In Section 3, we present the TRT steady recurrence equations and obtain the parametrization properties of TRT solutions. Section 4 describes the generic multi-reflection approach. Dirichlet velocity, pressure and mixed schemes are worked out in Sections 5 to 7, respectively. Section 8 discusses an application of the developed schemes with MRT models. Section 9 concludes the paper. The Chapman-Enskog analysis of the TRT model with the variable mass and force terms is presented in Appendix A. Pressure schemes are constructed in Appendices B. The correspondence of the present notations with those in [16] is given in Appendix C.

## 2 The TRT-model

### 2.1 Definitions

The unknown variable of the scheme is the  $Q$ -dimensional population vector  $f(\vec{r}, t) = \{f_q, q = 0, \dots, Q-1\}$ . The populations are initialized at time  $t = 0$  on the nodes  $\vec{r}$  of an equidistant  $d$ -dimensional computational mesh. Each component  $f_q$  undergoes the collision step and propagates to the site  $\vec{r} + \vec{c}_q$  according to its velocity  $\vec{c}_q$ . The velocity set contains  $Q$  vectors: one zero,  $\vec{C}_0 = \vec{0}$ , for the rest population, and  $Q-1$  non-zero ones,  $\vec{c}_q = \{c_{q\alpha}, \alpha = 1, \dots, d\}$ ,  $q = 1, \dots, Q-1$ , for the moving populations. We will assume  $d2Q9$ ,  $d3Q15$  and  $d3Q19$  cubic sets [41] where the velocity components  $c_{q\alpha}$  are either zero or  $\pm 1$ .

Since each moving velocity vector has an opposite one, any pair of populations with opposite velocities  $(\vec{c}_q, \vec{c}_{\bar{q}})$ , hereafter referred to as a *link*, can be decomposed into its symmetric (even) and anti-symmetric (odd) components:

$$f_q = f_q^+ + f_q^-, \quad f_q^\pm = \frac{1}{2}(f_q \pm f_{\bar{q}}) \quad \vec{c}_q = -\vec{c}_{\bar{q}}. \quad (2.1)$$

For the rest population,  $f_0 = f_0^+$ ,  $f_0^- = 0$ . Assuming that the equilibrium components  $e_q^\pm(\vec{r}, t)$  and an external source term  $S_q(\vec{r}, t) = S_q^-(\vec{r}, t) + S_q^+(\vec{r}, t)$  are prescribed, the time and space evolution of population solution is computed with the TRT linear collision

operator:

$$\begin{aligned} f_q(\vec{r}+\vec{c}_q, t+1) &= \tilde{f}_q(\vec{r}, t), \quad q=0, \dots, Q-1, \\ \tilde{f}_q(\vec{r}, t) &= f_q(\vec{r}, t) + p_q + m_q + S_q, \\ p_q &= \lambda_e n_q^+, \quad m_q = \lambda_o n_q^-, \quad n_q^\pm = f_q^\pm - e_q^\pm. \end{aligned} \quad (2.2)$$

The symmetric/antisymmetric components can be computed only once for each link:

$$\begin{aligned} f_q^+ &= f_{\bar{q}}^+, \quad f_q^- = -f_{\bar{q}}^-, \quad e_q^+ = e_{\bar{q}}^+, \\ e_q^- &= -e_{\bar{q}}^-, \quad p_q = p_{\bar{q}}, \quad m_q = -m_{\bar{q}}. \end{aligned} \quad (2.3)$$

They can be regarded as the population projections on the link-wise symmetric/antisymmetric orthogonal basis vectors of the  $Q$ -dimensional space. Two collision parameters, “even”  $\lambda_e$  and “odd”  $\lambda_o$ , are the eigenvalues of the linear collision operator in such a basis. The TRT collision operator can be regarded as a particular form of the multiple-relaxation-times (MRT) models [17, 19, 29, 31] when their eigenvalues, associated with the even and odd order polynomial MRT-basis vectors, are equal to  $\lambda_e$  and  $\lambda_o$ , respectively. The BGK model [41] is a TRT sub-class with a single relaxation parameter

$$\tau = -\frac{1}{\lambda_e} = -\frac{1}{\lambda_o}.$$

The linear stability of the evolution equation restricts the eigenvalues to the interval  $] -2, 0[$ . Note that we have removed  $-2$  and  $0$  from the stability interval. When one eigenvalue is zero, it appears a set of additional conserved quantities, thus additional macroscopic equations. In a similar way, the value  $-2$  corresponds to staggered conserved quantities not suitable for ordinary models. The following eigenvalue functions are then positive:

$$\Lambda_e = -\left(\frac{1}{2} + \frac{1}{\lambda_e}\right), \quad \Lambda_o = -\left(\frac{1}{2} + \frac{1}{\lambda_o}\right), \quad \Lambda_{eo} = \Lambda_e \Lambda_o. \quad (2.4)$$

In order to prescribe macroscopic mass source  $M(\vec{r}, t)$  and body-force  $\vec{F}(\vec{r}, t)$ , the local mass and momentum constraints are:

$$\sum_{q=0}^{Q-1} \tilde{f}_q(\vec{r}, t) = \sum_{q=0}^{Q-1} f_q(\vec{r}, t) + M(\vec{r}, t), \quad (2.5)$$

$$\sum_{q=1}^{Q-1} \tilde{f}_q(\vec{r}, t) \vec{c}_q = \sum_{q=1}^{Q-1} f_q(\vec{r}, t) \vec{c}_q + \vec{F}(\vec{r}, t), \quad (2.6)$$

where only the mass conservation constraints are considered for modeling advection-diffusion equations. Let us define the following microscopic mass and momentum quan-

tities from the local population  $f_q^\pm$ , equilibrium distributions  $e_q^\pm$ , and source terms  $S_q^\pm$ :

$$\begin{aligned}\rho &= \sum_{q=0}^{Q-1} f_q^+, & \vec{J} &= \sum_{q=1}^{Q-1} f_q^- \vec{c}_q, \\ \rho^{\text{eq}} &= \sum_{q=0}^{Q-1} e_q^+, & \vec{j}^{\text{eq}} &= \sum_{q=1}^{Q-1} e_q^- \vec{c}_q, \\ \mathcal{M} &= \sum_{q=0}^{Q-1} S_q^+, & \vec{\mathcal{F}} &= \sum_{q=1}^{Q-1} S_q^- \vec{c}_q,\end{aligned}\tag{2.7}$$

where  $\mathcal{M}$  and  $\vec{\mathcal{F}}$  represent the contributions coming from the selected local mass and momentum sources  $S_q^\pm$ . As shown below, the way  $M$  is split between  $\rho^{\text{eq}}$  and  $\mathcal{M}$ , and  $\vec{F}$  between  $\vec{j}^{\text{eq}}$  and  $\vec{\mathcal{F}}$ , is arbitrary. The solvability conditions of Eq. (2.2), derived from relations (2.5), (2.6), and the two relations in the last line of (2.7), are:

$$\begin{aligned}\sum_{q=0}^{Q-1} p_q(\vec{r}, t) &= M - \mathcal{M}, \\ \sum_{q=1}^{Q-1} m_q(\vec{r}, t) \vec{c}_q &= \vec{F} - \vec{\mathcal{F}}.\end{aligned}\tag{2.8}$$

Using then the definitions of  $p_q$  and  $m_q$ , the equilibrium variables are related to the microscopic mass and momentum by

$$\begin{aligned}\sum_{q=0}^{Q-1} p_q(\vec{r}, t) &= \lambda_e (\rho - \rho^{\text{eq}}), & \text{i.e., } \rho^{\text{eq}} &= \rho - \frac{M - \mathcal{M}}{\lambda_e}, \\ \sum_{q=1}^{Q-1} m_q(\vec{r}, t) \vec{c}_q &= \lambda_o (\vec{J} - \vec{j}^{\text{eq}}), & \text{i.e., } \vec{j}^{\text{eq}} &= \vec{J} - \frac{\vec{F} - \vec{\mathcal{F}}}{\lambda_o}.\end{aligned}\tag{2.9}$$

The redefinition of the macroscopic momentum  $\vec{j}$  with respect to the microscopic momentum  $\vec{J}$  in the presence of a forcing term has been discussed in [6, 13, 16, 24, 35]:

$$\vec{j} = \vec{J} + \frac{\vec{F}}{2}.\tag{2.10}$$

We show in Appendix A that in the presence of mass source terms, the macroscopic conserved mass variable  $\rho^m$  should also be redefined as:

$$\rho^m = \rho + \frac{M}{2}.\tag{2.11}$$

Therefore, the equilibrium variables are related to the macroscopic variables by:

$$\begin{aligned} \rho^{\text{eq}} &= \rho^m + \Lambda_e M + \frac{\mathcal{M}}{\lambda_e}, & \rho^m &= \rho + \frac{M}{2}, & \rho &= \sum_{q=0}^{Q-1} f_q = \sum_{q=0}^{Q-1} f_q^+, \\ \vec{j}^{\text{eq}} &= \vec{j} + \Lambda_o \vec{F} + \frac{\vec{\mathcal{F}}}{\lambda_o}, & \vec{j} &= \vec{J} + \frac{\vec{F}}{2}, & \vec{J} &= \sum_{q=1}^{Q-1} f_q \vec{c}_q = \sum_{q=1}^{Q-1} f_q^- \vec{c}_q. \end{aligned} \quad (2.12)$$

We emphasize that  $\mathcal{M}$  and  $\vec{\mathcal{F}}$  are defined with the last relations (2.7), via the choice of the mass,  $\{S_q^+\}$ , and momentum,  $\{S_q^-\}$ , source distributions. When  $\mathcal{M}$  and  $\vec{\mathcal{F}}$  are specified, the equilibrium variables are uniquely defined from the microscopic solutions obtained via relations (2.12). The converse is also true: the choice for  $\rho^{\text{eq}}$  and  $\vec{j}^{\text{eq}}$  uniquely defines  $\mathcal{M}$  and  $\vec{\mathcal{F}}$  via relations (2.9).

## 2.2 Hydrodynamic equilibrium and forcing

Relations (2.12) define a class of equivalent models. We describe one sub-class based on the isotropic equilibrium weights [41]. For the cubic velocity sets, these weights are uniquely defined by the following (isotropic) conditions:

$$\sum_{q=1}^{Q-1} t_q^* c_{q\alpha} c_{q\beta} = \delta_{\alpha\beta}, \quad \forall \alpha, \beta, \quad 3 \sum_{q=1}^{Q-1} t_q^* c_{q\alpha}^2 c_{q\beta}^2 = 1, \quad \alpha \neq \beta. \quad (2.13)$$

Based on the ideas in [26, 41], let us define the equilibrium as:

$$\begin{aligned} e_0^+ &= e_0 = \rho^{\text{eq}} - \sum_{q=1}^{Q-1} e_q^+, & e_q^+ &= t_q^* \Pi_q(\rho^{\text{eq}}, \vec{j}, \hat{\rho}), \quad q = 1, \dots, Q-1, \\ e_q^- &= t_q^* (\vec{j}^{\text{eq}} \cdot \vec{c}_q), & S_q^- &= t_q^* (\vec{\mathcal{F}} \cdot \vec{c}_q), \\ \Pi_q(\rho, \vec{j}, \hat{\rho}) &= c_s^2 \rho + g_s E_q^+(\vec{j}, \hat{\rho}), & E_q^+(\vec{j}, \hat{\rho}) &= \frac{3j_q^2 - \|\vec{j}\|^2}{2\hat{\rho}}, \\ S_q^+ &= c_s^2 t_q^* \mathcal{M}, & S_0^+ &= \mathcal{M} - \sum_{q=1}^{Q-1} S_q^+. \end{aligned} \quad (2.14)$$

We assume

$$g_s = 1, \quad \hat{\rho} = \rho^m \quad (\text{or } \hat{\rho} = \rho_0)$$

for modeling the compressible (incompressible, respectively) Navier-Stokes equations and  $g_s = 0$  for the Stokes equations. The sound velocity is  $0 < c_s < 1$  (further restrictions and optimal solutions come from the stability analysis, e.g., in [36]). Note that the equilibrium functions given in (2.14) are by no mean ‘‘approximations’’, but come from a deliberate choice motivated, first, because they are so far the most widely used, secondly, because they lead to simpler algebra, and finally, because they allow one to find

exact solutions. Indeed the derivations in the following sections can be applied to other equilibrium functions, such as the “entropic” equilibrium of [2].

As an example of the use of relations (2.9) to (2.12), the three following definitions result in equivalent TRT schemes once the external forcing  $\vec{F}$  is given:

$$\begin{aligned} \vec{j}^{\text{eq}} = \vec{j} = \vec{j} - \frac{1}{2}\vec{F}, \quad \vec{\mathcal{F}} = \vec{F}, \quad \sum_{q=1}^{Q-1} m_q \vec{c}_q = 0, \\ \vec{j}^{\text{eq}} = \vec{j}, \quad \vec{\mathcal{F}} = -\lambda_o \Lambda_o \vec{F}, \quad \sum_{q=1}^{Q-1} m_q \vec{c}_q = -\frac{\lambda_o}{2} \vec{F}, \\ \vec{j}^{\text{eq}} = \vec{j} - \frac{\vec{F}}{\lambda_o} = \vec{j} + \Lambda_o \vec{F}, \quad \vec{\mathcal{F}} = 0, \quad \sum_{q=1}^{Q-1} m_q \vec{c}_q = \vec{F}. \end{aligned} \quad (2.15)$$

The solutions of the TRT evolution equation using the equilibrium (2.14) with relations (2.15) are identical for  $f_q^\pm$  and  $p_q$  but not for  $m_q$ . With the help of the last relations (2.12) and for two equivalent equilibrium functions  $e_q^{-I}$  and  $e_q^{-II}$ , one obtains:

$$\begin{aligned} m_q^{(I)} - m_q^{(II)} &= \lambda_o (e_q^{-(II)} - e_q^{-(I)}) = t_q^* \lambda_o (j_q^{\text{eq}(II)} - j_q^{\text{eq}(I)}) \\ &= t_q^* ((\vec{\mathcal{F}}^{(II)} - \vec{\mathcal{F}}^{(I)}) \cdot \vec{c}_q) = S_q^{-(II)} - S_q^{-(I)}. \end{aligned} \quad (2.16)$$

For any pair  $\{\vec{j}^{\text{eq}}, S_q^-\}$  which obeys relations (2.12) the component  $m_q^{(F)}$  keeps the same value:

$$m_q^{(F)} = m_q + S_q^-, \quad q = 1, \dots, Q-1. \quad (2.17)$$

The first setup in (2.15) keeps the momentum conserving equilibrium function, following the MRT convention [13, 16]. The second setup equates  $\vec{j}^{\text{eq}}$  to the macroscopic variable  $\vec{j}$ , as the BGK model in [6, 24]. This setup simplifies the analysis of the Dirichlet boundary conditions which are prescribed for  $\vec{j}$  and not for  $\vec{j}^{\text{eq}}$ . The third setup includes the source terms into the equilibrium. This avoids an extra construction of the source gradients when deriving the population solution. One can construct equivalent schemes based on the different definitions for  $\rho^{\text{eq}}$  and the mass source  $\mathcal{M}$ , e.g.:

$$\begin{aligned} \rho^{\text{eq}} = \rho = \rho^m - \frac{1}{2}M, \quad \mathcal{M} = M, \quad \sum_{q=0}^{Q-1} p_q = 0, \\ \rho^{\text{eq}} = \rho^m, \quad \mathcal{M} = -\lambda_e \Lambda_e M, \quad \sum_{q=0}^{Q-1} p_q = -\frac{\lambda_e}{2} M, \\ \rho^{\text{eq}} = \rho - \frac{M}{\lambda_e} = \rho^m + \Lambda_e M, \quad \mathcal{M} = 0, \quad \sum_{q=0}^{Q-1} p_q = M. \end{aligned} \quad (2.18)$$

The solutions are then identical for  $f_q^\pm$ , and therefore for  $\vec{j}$  and  $\rho^m$ . With the help of the last relations (2.12), one obtains

$$\begin{aligned} p_q^{(I)} - p_q^{(II)} &= \lambda_e (e_q^{+(II)} - e_q^{+(I)}) = t_q^* c_s^2 \lambda_e (\rho^{\text{eq}(II)} - \rho^{\text{eq}(I)}) \\ &= S_q^{+(II)} - S_q^{+(I)}, \quad q=0, \dots, Q-1. \end{aligned} \quad (2.19)$$

Then for any equivalent choice of  $\rho^{\text{eq}}$  and  $S_q^+$ , the component  $p_q^{(M)}$  keeps the same value:

$$p_q^{(M)} = p_q + S_q^+, \quad q=0, \dots, Q-1. \quad (2.20)$$

Inspired by the idea of the Chapman-Enskog expansion, relations (A.2) in Appendix A express  $n_q^\pm$  in terms of the gradients of the equilibrium components. The macroscopic equations are identical for any choice of the source terms  $S_q^\pm$  provided that relations (2.12) are obeyed. Using the notations:

$$\begin{aligned} \Pi_q^* &= t_q^* \Pi_q, & M_q^* &= c_s^2 t_q^* M, & F_q^* &= t_q^* F_q, & F_q &= (\vec{F} \cdot \vec{c}_q), \\ j_q^* &= t_q^* j_q, & j_q &= (\vec{j} \cdot \vec{c}_q), & j_q^{\text{eq}*} &= t_q^* j_q^{\text{eq}}, & j_q^{\text{eq}} &= (\vec{j}^{\text{eq}} \cdot \vec{c}_q), \end{aligned} \quad (2.21)$$

the third-order accurate TRT solution (A.11) for *incompressible flow* becomes:

$$\begin{aligned} n_q^+ &= \frac{p_q}{\lambda_e}, & n_q^- &= \frac{m_q}{\lambda_o}, \\ p_q &= p_q^{(1)} + p_q^{(2)} + \mathcal{O}(\varepsilon^3) = p_q^{(M)} - S_q^+, \\ m_q &= m_q^{(1)} + m_q^{(2)} + \mathcal{O}(\varepsilon^3) = m_q^{(F)} - S_q^-, \\ p_q^{(M)} &= \partial_q j_q^* + \partial_t \Pi_q^* - \partial_q \Lambda_o (\partial_q \Pi_q^* - F_q^*) - \partial_q \Lambda_{eo} \partial_q M_q^* + \Lambda_e \partial_t M_q^*, \\ m_q^{(F)} &= \partial_q \Pi_q^* + \partial_t j_q^* - \partial_q \Lambda_e (\partial_q j_q^* - M_q^*) - \partial_q \Lambda_{eo} \partial_q F_q^* + \Lambda_o \partial_t F_q^*. \end{aligned} \quad (2.22)$$

These relations can be viewed as a restriction of the Chapman-Enskog expansion (A.2) to the “diffusive time scaling expansion” (see last relations in Appendix A), without any additional assumption on the asymptotic behavior of the equilibrium and source components. Hereafter we omit the mass source for simplicity.

When the population expansion (2.22) is matched exactly for  $\mathcal{O}(\partial_q^{(n-1)} j_q^*)$ ,  $\mathcal{O}(\partial_q^{(k-1)} \Pi_q^*)$  and  $\mathcal{O}(\partial_q^{(l-1)} F_q^*)$  terms, we will say then that the accuracy of a given boundary scheme is represented by the triplet

$$j^{(n)} / \Pi^{(k)} / F^{(l)}. \quad (2.23)$$

We will refer to schemes with the triplet  $j^{(2)} / \Pi^{(1)} / F^{(0)}$  as “linear” or “second-order” schemes and with the triplet  $j^{(3)} / \Pi^{(2)} / F^{(1)}$  as “parabolic” or “third-order” schemes, respectively. The linear schemes are exact, at least when  $g_S=0$ , for linear flows and uniform

pressure (typically, a Couette flow) and the parabolic schemes are exact for parabolic velocity profiles and linear pressure distributions (and/or uniform force distribution), as a Poiseuille Stokes flow in arbitrarily inclined channels. As a further example, we construct  $j^{(3)}/\Pi^{(3)}/F^{(2)}$  schemes which are exact for linear velocity/forcing and parabolic pressure solutions for Navier-Stokes equation, see [33]. The focus is on the development of pressure and velocity schemes of equivalent accuracy, their adaptation for corners, the study of their parametrization properties for steady problems, their support of the staggered solutions and the analysis of their effective accuracy for time dependent boundary conditions.

### 3 TRT steady solutions

For the sake of simplicity, we follow the third set-up in relations (2.15) and (2.18) and set here  $S_q^\pm = 0$ . Including the source variables into the equilibrium allows us to get their gradients in expansion as for the equilibrium variables.

#### 3.1 Infinite steady expansion

Based on a parity argument only and the idea of the Chapman [8] and Enskog [10] to represent a solution as its expansion around *the local equilibrium*, the steady solution to TRT operator can be given as infinite series:

$$\begin{aligned}
 n_q^+ &= \sum_{k \geq 1} n_q^{+(k)}, & n_q^- &= \sum_{k \geq 1} n_q^{-(k)}, \\
 n_q^{+(k)} &= \frac{p_q^{(k)}}{\lambda_e}, & n_q^{-(k)} &= \frac{m_q^{(k)}}{\lambda_o}, & k \geq 1, \\
 n_q^{+(0)} &= e_q^+, & n_q^{-(0)} &= e_q^-, \\
 p_q^{(k)} &= \sum_{\substack{r=2s-1 \\ 1 \leq s \leq \frac{k+1}{2}}} \frac{\partial_q^r n_q^{-(k-r)}}{r!} + \sum_{\substack{r=2s \\ 1 \leq s \leq \frac{k}{2}}} \frac{\partial_q^r n_q^{+(k-r)}}{r!}, \\
 m_q^{(k)} &= \sum_{\substack{r=2s-1 \\ 1 \leq s \leq \frac{k+1}{2}}} \frac{\partial_q^r m_q^{+(k-r)}}{r!} + \sum_{\substack{r=2s \\ 1 \leq s \leq \frac{k}{2}}} \frac{\partial_q^r m_q^{-(k-r)}}{r!}.
 \end{aligned} \tag{3.1}$$

When  $k=2$ , the solution reduces to relations (2.22) where the time derivatives have been dropped.

### 3.2 Recurrence equations

Assuming that  $\lambda_o$  and  $\lambda_e$  are constant in space and time, an equivalent link-wise “finite-difference” form of the TRT evolution equation is (the derivation is reported in [32]):

$$\begin{aligned} p_q &= \lambda_e n_q^+ = \bar{\Delta}_q e_q^- - \Lambda_o \Delta_q^2 e_q^+ + (\Lambda_{eo} - \frac{1}{4}) \Delta_q^2 p_q, \\ m_q &= \lambda_o n_q^- = \bar{\Delta}_q e_q^+ - \Lambda_e \Delta_q^2 e_q^- + (\Lambda_{eo} - \frac{1}{4}) \Delta_q^2 m_q, \end{aligned} \quad (3.2)$$

where

$$\begin{aligned} \bar{\Delta}_q \phi(\vec{r}) &= \frac{1}{2} (\phi(\vec{r} + \vec{c}_q) - \phi(\vec{r} - \vec{c}_q)), \\ \Delta_q^2 \phi(\vec{r}) &= \phi(\vec{r} + \vec{c}_q) - 2\phi(\vec{r}) + \phi(\vec{r} - \vec{c}_q), \quad \forall \phi. \end{aligned} \quad (3.3)$$

Together with the solvability relations (2.8), the recurrence Eqs. (3.2) give a system of equations for the variables  $\{p_q, m_q\}$  and the unknown equilibrium quantities (e.g.,  $\rho$  and  $\vec{J}$  for hydrodynamic models). Other linear combinations of the TRT equations relate the  $p_q$  and  $m_q$ :

$$\begin{aligned} \Delta_q^2 e_q^+ - \Lambda_e \Delta_q^2 p_q - \bar{\Delta}_q m_q &= 0, \\ \Delta_q^2 e_q^- - \Lambda_o \Delta_q^2 m_q - \bar{\Delta}_q p_q &= 0. \end{aligned} \quad (3.4)$$

Based on the parity argument and the linearity of the recurrence equations with respect to the equilibrium components, we look for solution in the form

$$\begin{aligned} p_q(e_q^+, e_q^-) &= p_q(e_q^-) - 2\Lambda_o p_q(e_q^+), \\ m_q(e_q^+, e_q^-) &= m_q(e_q^+) - 2\Lambda_e m_q(e_q^-). \end{aligned} \quad (3.5)$$

Expanding  $p_q(e_q^\pm)$  and  $m_q(e_q^\pm)$  around their equilibrium values, the *exact explicit solution* for all their coefficients in the series is obtained in [32] from the recurrence equations (3.5). It tells us that the coefficients of  $p_q(e_q^\pm)$  and  $m_q(e_q^\pm)$  depend on the eigenvalue functions  $\Lambda_o$  and  $\Lambda_e$  only via their combination  $\Lambda_{eo}$ . Substituting the obtained series into relations (3.5) one can show, with the help of relations (3.4), that the infinite steady expansion (3.1) and the solution of the recurrence equations coincide for both non-equilibrium components.

### 3.3 Dimensional and parametrization properties of the bulk solutions

The hydrodynamic solutions are determined via the non-dimensional numbers: Mach number  $Ma$ , Froude number  $Fr$  and Reynolds number  $Re$ :

$$Ma = \frac{U}{c_s}, \quad Fr = \frac{U^2}{gL}, \quad Re = \frac{UL}{\nu}, \quad (3.6)$$

with some characteristic acceleration parameter, e.g., the gravitation constant  $g$  if  $\vec{F} = \rho_0 g$ . Let us introduce the dimensionless variables

$$\vec{j}' = \frac{\vec{j}}{\rho_0 U'}, \quad P' = \frac{P - P_0}{\rho_0 U'^2}, \quad \hat{\rho}' = \frac{\hat{\rho}}{\rho_0}, \quad \vec{F}' = \frac{FrL}{\rho_0 U'^2} \vec{F},$$

where  $P = c_s^2 \rho$ ,  $P_0 = c_s^2 \rho_0$ ,  $\forall \rho_0$ , then

$$\begin{aligned} \rho' &= \frac{\rho}{\rho_0} = 1 + Ma^2 P', \\ \Pi'_q(\rho', \vec{j}', \hat{\rho}') &= \frac{\Pi_q(\rho, \vec{j}, \hat{\rho})}{\rho_0 U'^2} = Ma^{-2} + P' + E_q^+(\vec{j}', \hat{\rho}'). \end{aligned} \quad (3.7)$$

Using the notations:  $j'_q{}^* = t_q^*(\vec{j}' \cdot \vec{c}_q)$ ,  $\Pi'_q{}^* = t_q^* \Pi'_q$ ,  $F'_q{}^* = t_q^*(\vec{F}' \cdot \vec{c}_q)$ , we express the solution (3.5) in terms of the dimensionless variables and present them in an equivalent form:

$$\begin{aligned} \frac{L}{\rho_0 U} p_q &= L p_q(j'_q{}^*) - 2\Lambda_o U L p_q(\Pi'_q{}^*) + \frac{\Lambda_o U}{Fr} p_q(F'_q{}^*), \\ \frac{L}{\rho_0 U^2} m_q^{(F)} &= L m_q(\Pi'_q{}^*) - \frac{2\Lambda_e L}{U} m_q(j'_q{}^*) - \frac{2\Lambda_{eo}}{Fr} m_q(F'_q{}^*). \end{aligned} \quad (3.8)$$

Substituting relations (3.8) into the exact mass and momentum conservation relations (2.8), with

$$\sum_{q=0}^{Q-1} p_q = 0, \quad \sum_{q=1}^{Q-1} m_q^{(F)} \vec{c}_q = \vec{F},$$

one obtains the exact steady state conservation relations as

$$\begin{aligned} 3L \sum_{q=0}^{Q-1} p_q(j'_q{}^*) &= 2\Lambda_{eo} Re \sum_{q=0}^{Q-1} p_q(\Pi'_q{}^*) + \frac{\Lambda_{eo}}{L} \frac{Re}{Fr} \sum_{q=0}^{Q-1} p_q(F'_q{}^*), \\ L \sum_{q=1}^{Q-1} m_q(\Pi'_q{}^*) \vec{c}_q &= \frac{\vec{F}'}{Fr} + \frac{6L^2}{Re} \sum_{q=1}^{Q-1} m_q(j'_q{}^*) \vec{c}_q + \frac{2\Lambda_{eo}}{Fr} \sum_{q=1}^{Q-1} m_q(F'_q{}^*) \vec{c}_q. \end{aligned} \quad (3.9)$$

It is noted that all the non-equilibrium components in relations (3.9) depend on  $\Lambda_e$  and  $\Lambda_o$  only via their combination  $\Lambda_{eo}$ . When  $g_s = 1$ ,  $\hat{\rho} = \rho_0$ , then the solutions for  $\vec{j}'$  and  $P'$  are *identical on a given grid (L fixed)* for any  $\Lambda_e$ ,  $\Lambda_o$ ,  $\rho_0$ ,  $g$  and  $U$  provided that  $Re$ ,  $Fr$  and  $\Lambda_{eo}$  are fixed. In the compressible regime,  $\hat{\rho} = \rho$  and  $Ma$  should be fixed additionally. These results, based on the truncated second-order expansion (2.22), mean that the hydrodynamic parts of the exact mass and momentum conservation equations (A.10) are controlled by the hydrodynamic numbers in steady and transient regimes. However, the higher-order corrections to these equations depend on  $\Lambda_{eo}$  only.

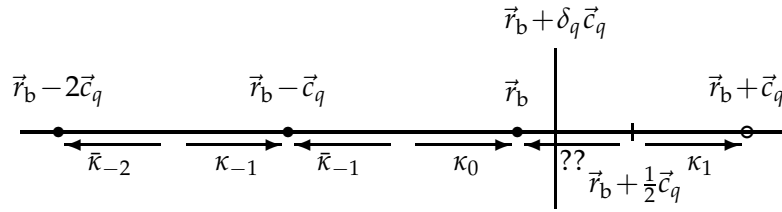


Figure 1: The velocity  $\vec{c}_q$  cuts the boundary surface at  $\vec{r}_b + \delta_q \vec{c}_q$ , between the boundary node  $\vec{r}_b$  and an outside node  $\vec{r}_b + \vec{c}_q$ . The figure is recalled from [16].

For the Stokes equilibrium ( $g_S = 0$ ), any steady solution  $v\vec{j}(\vec{r})$  does not depend then on  $\Lambda_e$  and  $\Lambda_o$  separately but only on their combination  $\Lambda_{eo}$ . Assuming the Darcy law for the mean value  $\vec{j}$ ,

$$v\vec{j} = \mathbf{K}(\vec{F} - \nabla P), \tag{3.10}$$

and setting  $\Lambda_{eo}$  to some given value, the components of the permeability tensor  $\mathbf{K}$  will yield the same solution, independently from the selected viscosity and forcing values. When the exact microscopic rules set by the boundary schemes are parameterized as the steady bulk conservation relations, the numerical solutions carry the bulk properties *exactly* for the Stokes and Navier-Stokes regimes.

Finally, we emphasize that for transient flows only the spatial part of the population solution is controlled by  $\Lambda_{eo}$  and that the higher-order corrections to the macroscopic equations depend on both  $\Lambda_e$  and  $\Lambda_o$ .

## 4 Multi-reflection (MR) type boundary condition

### 4.1 Generic $M_q$ -scheme

We assume that  $\vec{r}_b$  is an *inside* boundary node and that  $\vec{r}_w$ ,

$$\vec{r}_w = \vec{r}_b + \delta_q \vec{c}_q, \quad 0 \leq \delta_q \leq 1,$$

is the point where  $\vec{c}_q$  intersects the wall (see Fig. 1). We refer to  $\vec{c}_q$  as a “cut link” and  $\Pi^c(\vec{r}_b)$  is the set of all the cut links at  $\vec{r}_b$ . It is split in  $\Pi^{(u)}(\vec{r}_b)$ , for the velocities cutting the boundary  $\Gamma^{(u)}$  where Dirichlet velocity conditions are imposed, and  $\Pi^{(p)}(\vec{r}_w)$ , for the velocities cutting the boundary  $\Gamma^{(p)}$  where the mixed (pressure/tangential velocity) conditions are imposed:

$$\Pi^c(\vec{r}_b) = \Pi^{(u)}(\vec{r}_b) \cup \Pi^{(p)}(\vec{r}_w).$$

Any link which bisects both boundaries is assigned to one of these two boundary conditions in this paper (see sketch on Fig. 2). More complicated situations are possible but not

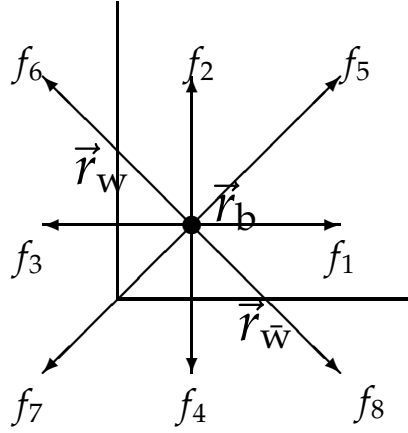


Figure 2: An example of a “corner” node  $\vec{r}_b$  on  $d2Q9$  grid. Second-type link is  $\{\vec{c}_6, \vec{c}_8\}$ . We assume that the link going through the corner,  $\vec{c}_7$ , either belongs to  $\Pi^{(p)}(\vec{r}_b)$  or to  $\Pi^{(u)}(\vec{r}_b)$  but not to both at the same time.

considered here for simplicity. Multi-reflection [16, 18] involves five post-collision neighboring values for each unknown population  $f_q(\vec{r}_b, t+1)$ . Here, we first write down their combination  $R_q(\vec{r}_b, t)$  with the free coefficients  $\kappa_1, \kappa_0, \kappa_{-1}, \bar{\kappa}_{-1}, \bar{\kappa}_{-2}$  and two additional terms  $f_q^{\text{p.c.}}(\vec{r}_b, t)$  and  $w_q(\vec{r}_w, t)$ :

$$\begin{aligned}
 f_q(\vec{r}_b, t+1) &= M_q(\vec{r}_b, t), \\
 M_q(\vec{r}_b, t) &= R_q(\vec{r}_b, t) + f_q^{\text{p.c.}}(\vec{r}_b, t) + w_q(\vec{r}_w, t), \\
 R_q(\vec{r}_b, t) &= \kappa_1 \tilde{f}_q(\vec{r}_b, t) + \kappa_0 \tilde{f}_q(\vec{r}_b - \vec{c}_q, t) + \kappa_{-1} \tilde{f}_q(\vec{r}_b - 2\vec{c}_q, t) \\
 &\quad + \bar{\kappa}_{-1} \tilde{f}_q(\vec{r}_b, t) + \bar{\kappa}_{-2} \tilde{f}_q(\vec{r}_b - \vec{c}_q, t), \quad q \in \Pi^c(\vec{r}_b).
 \end{aligned} \tag{4.1}$$

An equivalent *two-point* form for  $R_q(\vec{r}_b, t)$  is:

$$\begin{aligned}
 R_q(\vec{r}_b, t) &= \kappa_1 \tilde{f}_q(\vec{r}_b, t) + \kappa_0 f_q(\vec{r}_b, t+1) + \bar{\kappa}_{-1} \tilde{f}_q(\vec{r}_b, t) \\
 &\quad + \kappa_{-1} f_q(\vec{r}_b - \vec{c}_q, t+1) + \bar{\kappa}_{-2} \tilde{f}_q(\vec{r}_b - \vec{c}_q, t).
 \end{aligned} \tag{4.2}$$

In the next sections, we develop the  $M_q^{(u)}$  schemes (5.2) for Dirichlet velocity conditions and the  $M_q^{(p)}$  schemes (6.2) for Dirichlet pressure conditions. Their coefficients and  $f_q^{\text{p.c.}}$  corrections are defined in Tables 3 and 9, respectively. The mixed scheme  $M_q^{(m)}$  combines velocity and pressure schemes in Section 7.

## 4.2 Special links with $M_q$

One can distinguish two types of links with potential difficulties to compute  $R_q$  in relations (4.1). The *first type* of special links cannot define  $\kappa_{-1} \tilde{f}_q(\vec{r}_b - 2\vec{c}_q, t)$  when the point  $(\vec{r}_b - 2\vec{c}_q)$  lies outside the computational grid. Keeping in mind the equivalent

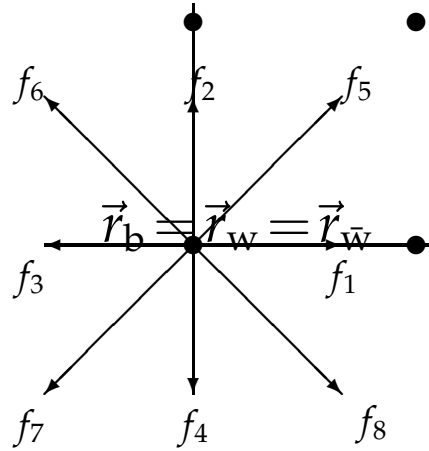


Figure 3: Second-type link  $\{\vec{c}_6, \vec{c}_8\}$  cuts the wall at grid “corner” vertex  $\vec{r}_b = \vec{r}_w = \vec{r}_{\bar{w}}$ .

two-point form (4.2), we replace  $\kappa_{-1}f_q(\vec{r}_b - \vec{c}_q, t+1)$  by the previous time step solution,  $\kappa_{-1}f_q(\vec{r}_b - \vec{c}_q, t)$ . Such a substitution yields the same *steady* solution. Another technique we use is to switch the three points scheme to a two-point one, equivalent (similar) in accuracy but with  $\kappa_{-1} = 0$ .

When both neighbors  $(\vec{r}_b \pm \vec{c}_q)$  lie outside the computational grid,  $\{\vec{c}_q, \vec{c}_{\bar{q}}\} \in \Pi^c(\vec{r}_b)$ , this *second type* of special links cannot use  $\kappa_0 \tilde{f}_q(\vec{r}_b - \vec{c}_q, t+1)$  nor  $\bar{\kappa}_{-2} \tilde{f}_{\bar{q}}(\vec{r}_b - \vec{c}_q, t)$ . This situation is typical when one link bisects two adjacent faces (see sketch on Fig. 2), hereafter referred to as a “corner” node. Link-wise conditions are then restricted to 1–3 population schemes where  $\kappa_{-1} = 0$ ,  $\bar{\kappa}_{-2} = 0$ , and replacing  $\kappa_0 \tilde{f}_q(\vec{r}_b - \vec{c}_q, t+1)$  with  $\kappa_0 f_q(\vec{r}_b, t)$ :

$$R_q(\vec{r}_b, t) = \kappa_1 \tilde{f}_q(\vec{r}_b, t) + \kappa_0 f_q(\vec{r}_b, t) + \bar{\kappa}_{-1} \tilde{f}_{\bar{q}}(\vec{r}_b, t) + f_q^{p.c.}(\vec{r}_b, t). \tag{4.3}$$

We discuss below how local “corner” schemes (4.3) can maintain third-order accuracy for the second-type links with the help of  $f_q^{p.c.}(\vec{r}_b, t)$ .

### 4.3 Exact MR closure relations

They are stated by relations (4.1). Dropping hereafter mass source variable, we substitute there:

$$\begin{aligned} f_q(\vec{r}, t) &= [e_q^+ + e_q^- + \frac{p_q}{\lambda_e} + \frac{m_q}{\lambda_o}](\vec{r}, t), \quad \vec{r} = \{\vec{r}_b, \vec{r}_b - \vec{c}_q, \vec{r}_b - 2\vec{c}_q\}, \quad \forall t, \\ f_{\bar{q}}(\vec{r}, t) &= [e_q^+ - e_q^- + \frac{p_q}{\lambda_e} - \frac{m_q}{\lambda_o}](\vec{r}, t+1), \\ \tilde{f}_q(\vec{r}, t) &= [e_q^+ + e_q^- + p_q(1 + \frac{1}{\lambda_e}) + m_q(1 + \frac{1}{\lambda_o}) + S_q^-](\vec{r}, t), \\ \tilde{f}_{\bar{q}}(\vec{r}, t) &= [e_q^+ - e_q^- + p_q(1 + \frac{1}{\lambda_e}) - m_q(1 + \frac{1}{\lambda_o}) - S_q^-](\vec{r}, t). \end{aligned} \tag{4.4}$$

One gets then exact two-time ( $t$  and  $t+1$ ) boundary constraint on the equilibrium and the non-equilibrium components along a given link. The sufficient conditions on the coefficients, which enforce the *exact* microscopic rules to yield bulk parametrization properties at steady state, are examined for these relations in the next section. In Section 4.4, the coefficients  $\kappa_1 - \bar{\kappa}_{-2}$  and the terms  $f_q^{\text{p.c.}}(\vec{r}_b, t)$ ,  $w_q(\vec{r}_w, \hat{t})$  are defined such that the Taylor approximation in space of the exact closure relation fits the prescribed pressure/velocity Dirichlet values. We examine then the leading accuracy of the obtained schemes for time dependent boundary conditions.

### 4.3.1 Parametrization properties of the exact closure relations

The dimensional analysis from Section 3.3 works *exactly* when the *exact closure relations* keep the parametrization properties for all cut links. For steady solutions, it is simpler to work with the two-point form (4.2). Substituting there the solution (4.4) and dropping the time we get

$$\begin{aligned} & \sum_{r=\{\vec{r}_b, \vec{r}_b - \vec{c}_q\}} [A^{(u)} j_q^* + A^{(p)} \Pi_q^* + B^{(u)} p_q + B^{(p)} m_q^{(F)} + B^{(f)} F_q^*](\vec{r}) \\ &= -f_q^{\text{p.c.}}(\vec{r}_b) - w_q(\vec{r}_w), \end{aligned} \quad (4.5)$$

where

$$\begin{aligned} A^{(u)}(\vec{r}_b) &= \kappa_1 - \bar{\kappa}_{-1} + \kappa_0 + 1, & A^{(u)}(\vec{r}_b - \vec{c}_q) &= \kappa_{-1} - \bar{\kappa}_{-2}, \\ A^{(p)}(\vec{r}_b) &= \kappa_1 + \bar{\kappa}_{-1} + \kappa_0 - 1, & A^{(p)}(\vec{r}_b - \vec{c}_q) &= \kappa_{-1} + \bar{\kappa}_{-2}, \\ B^{(u)}(\vec{r}_b) &= (\kappa_1 + \bar{\kappa}_{-1}) + \frac{\kappa_1 + \bar{\kappa}_{-1} + \kappa_0 - 1}{\lambda_e}, & B^{(u)}(\vec{r}_b - \vec{c}_q) &= \bar{\kappa}_{-2} + \frac{\kappa_{-1} + \bar{\kappa}_{-2}}{\lambda_e}, \\ B^{(p)}(\vec{r}_b) &= (\kappa_1 - \bar{\kappa}_{-1}) + \frac{\kappa_1 - \bar{\kappa}_{-1} + \kappa_0 + 1}{\lambda_o}, & B^{(p)}(\vec{r}_b - \vec{c}_q) &= -\bar{\kappa}_{-2} + \frac{\kappa_{-1} - \bar{\kappa}_{-2}}{\lambda_o}, \\ B^{(f)}(\vec{r}_b) &= \Lambda_o A^{(u)}(\vec{r}_b), & B^{(f)}(\vec{r}_b - \vec{c}_q) &= \Lambda_o A^{(u)}(\vec{r}_b - \vec{c}_q). \end{aligned} \quad (4.6)$$

When  $f_q^{\text{p.c.}}(\vec{r}_b)$  is a linear combination of  $p_q(\vec{r}_b)$ ,  $m_q^{(F)}(\vec{r}_b)$  and  $F_q^*(\vec{r}_b)$ , their coefficients have to be added to  $B^{(u)}(\vec{r}_b)$ ,  $B^{(p)}(\vec{r}_b)$  and  $B^{(f)}(\vec{r}_b)$ , respectively. We substitute then the solution in the form (3.5) for  $m_q^{(F)}$  and  $p_q$  into relation (4.5) and reorganize it with respect to the non-dimensional solutions  $\vec{j}$  and  $P'$ . Taking into account that steady solutions  $p_q(e_q^\pm)$  and  $m_q(e_q^\pm)$  depend on the eigenvalues only via  $\Lambda_{eo}$ , we get the sufficient conditions as:

$$\begin{aligned} A^{(u)}(\vec{r}) &= r_1(\Lambda_{eo}, \vec{r}, q), & B^{(u)}(\vec{r}) &= r_2(\Lambda_{eo}, \vec{r}, q), \\ A^{(p)}(\vec{r}) &= \Lambda_o r_3(\Lambda_{eo}, \vec{r}, q), & B^{(p)}(\vec{r}) &= \Lambda_o r_4(\Lambda_{eo}, \vec{r}, q). \end{aligned} \quad (4.7)$$

Here,  $r_i(\Lambda_{eo}, \vec{r}, q)$  abbreviates any function which depends on the eigenvalues only via  $\Lambda_{eo}$  or does not depend on them. It is noted that  $r_i$  may depend on  $\delta_q$  and may differ for any two coefficients, from one point to another one, or from link to link. When the

Table 1: The *LHS* of the MR-closure relation is the linear combination of the elements on the first and third lines, with the coefficients from the second and fourth lines, respectively. The first two lines come from the Taylor expansion in space and time of the equilibrium components with respect to  $(\vec{r}_b, t)$ . The last two lines come from the directional Taylor expansion of  $m_q(\vec{r})$ ,  $p_q(\vec{r})$ , and  $S_q^-(\vec{r})$ . The *RHS*  $= -f_q^{\text{p.c.}}(\vec{r}_b, t) - w_q(\vec{r}_w, \hat{t})$ .

$e_q^+$	$\partial_q e_q^+$	$\partial_q^2 e_q^+$	$\partial_t e_q^+$	$e_q^-$	$\partial_q e_q^-$	$\partial_q^2 e_q^-$	$\partial_t e_q^-$
$\alpha^{(p)}$	$B^+$	$C^+$	-1	$\alpha^{(u)}$	$B^-$	$C^-$	1
$p_q$	$m_q$	$\partial_q p_q$	$\partial_q m_q$	$S_q^-$	$\partial_q S_q^-$	$\partial_q^2 S_q^-$	
$D^+$	$D^-$	$E^+$	$E^-$	$\alpha^{(u)} - 1$	$B^-$	$C^-$	

sufficient conditions are all satisfied, the steady solution on the given grid for  $\vec{j}$  and  $P'$  is fully determined by the choice of the hydrodynamic numbers and  $\Lambda_{eo}$ , for the Navier-Stokes equilibrium. For the Stokes equilibrium, the solution for  $v\vec{j}$  is then fixed by  $\Lambda_{eo}$  and the forcing. Below, we will verify if the velocity/pressure schemes maintain the parametrization properties (4.7) exactly or at least up to a specific order.

#### 4.4 Approximated MR closure relations

With the goal of finding the coefficients of the multi-reflection, we replace the solution (4.4) in the exact closure relation with its Taylor approximation in space and time with respect to  $(\vec{r}_b, t)$ . More precisely, third-order accurate, directional in space and second-order accurate in time Taylor approximations are used for  $e_q^\pm(\vec{r}, t)$ . Assuming incompressible flow and in agreement with the diffusive scale expansion (2.22), the time variation is neglected for  $p_q(\vec{r}_b, t)$  and  $m_q(\vec{r}_b, t)$  and their space approximation is restricted to second-order. The obtained microscopic rule is referred to as the *approximated MR closure relation*. Its left-hand-side ( $LHS = R_q(\vec{r}_b, t) - f_q(\vec{r}_b, t+1)$ ) is equal to a linear combination of the elements presented in the first and third lines in Table 1. The *RHS* is equal to  $-f_q^{\text{p.c.}}(\vec{r}_b, t) - w_q(\vec{r}_w, \hat{t})$ . The coefficients of the *LHS* are presented by the elements from the second and fourth lines, respectively, with

$$\begin{aligned}
 A^+ &= \kappa_1 + \kappa_0 + \bar{\kappa}_{-1} + \kappa_{-1} + \bar{\kappa}_{-2}, & A^- &= -2(\bar{\kappa}_{-1} + \bar{\kappa}_{-2}), \\
 \alpha^{(p)} &= A^+ - 1, & \alpha^{(u)} &= A^+ + A^- + 1, \\
 B^+ &= -(\kappa_0 + 2\kappa_{-1} + \bar{\kappa}_{-2}), & B^- &= -(\kappa_0 + 2\kappa_{-1} - \bar{\kappa}_{-2}), \\
 C^+ &= \frac{1}{2}(\kappa_0 + 4\kappa_{-1} + \bar{\kappa}_{-2}), & C^- &= \frac{1}{2}(\kappa_0 + 4\kappa_{-1} - \bar{\kappa}_{-2}), \\
 D^+ &= (\alpha^{(p)} + 1) + \frac{\alpha^{(p)}}{\lambda_e}, & D^- &= (\alpha^{(u)} - 1) + \frac{\alpha^{(u)}}{\lambda_o}, \\
 E^+ &= B^+ \left(1 + \frac{1}{\lambda_e}\right), & E^- &= B^- \left(1 + \frac{1}{\lambda_o}\right).
 \end{aligned} \tag{4.8}$$

The closure relation is valid for any equilibrium function. We substitute then the hydrodynamic equilibrium (2.14) with (2.12) and the solution (2.22) for  $p_q$  and  $m_q$ , dropping the mass term and the second-order force gradients there. The simplest equivalent technique is to put  $\vec{\mathcal{F}}$  equal to zero in relation (2.12). The *LHS* of the obtained closure relation

Table 2: The LHS of the MR-closure relation is expressed in terms of the equilibrium gradients. It is given by the linear combination of the elements in the first line with the coefficients from the second line. The  $RHS = -f_q^{p.c.}(\vec{r}_b, t) - w_q(\vec{r}_w, \hat{t})$ .

$\Pi_q^*$	$\partial_q \Pi_q^*$	$\partial_q^2 \Pi_q^*$	$\partial_t \Pi_q^*$	$j_q^*$	$\partial_q j_q^*$	$\partial_q^2 j_q^*$	$\partial_t j_q^*$	$F_q^*$	$\partial_q F_q^*$	$\partial_t F_q^*$
$\alpha^{(p)}$	$\beta^{(p)}$	$\gamma^{(p)}$	$D^+ - 1$	$\alpha^{(u)}$	$\beta^{(u)}$	$\gamma^{(u)}$	$D^- + 1$	$\beta^{(f)}$	$\gamma^{(f)}$	$(D^- + 1)\Lambda_o$

represents then a linear combination of the elements given in the first line of Table 2, with the coefficients from the second line. The coefficients are given by relations (4.8) and their combinations:

$$\begin{aligned}
 \beta^{(p)} &= B^+ + D^-, & \beta^{(u)} &= B^- + D^+, \\
 \gamma^{(p)} &= C^+ - \Lambda_o D^+ + E^-, & \gamma^{(u)} &= C^- - \Lambda_e D^- + E^+, \\
 \beta^{(f)} &= \alpha^{(u)} \Lambda_o, & \gamma^{(f)} &= \beta^{(u)} \Lambda_o.
 \end{aligned}
 \tag{4.9}$$

The approximated closure relation is adapted for velocity and pressure conditions in the two next sections.

## 5 $M_q^{(u)}$ – schemes for Dirichlet velocity condition

### 5.1 Principal schemes

We assume that the velocity distribution is prescribed on  $\Gamma^{(u)}$ :

$$\vec{u}(\vec{r}_b + \delta_q \vec{c}_q, t) = \vec{u}^b(\vec{r}_w, t), \quad \vec{r}_w \in \Gamma^{(u)}, \quad q \in \Pi^{(u)}(\vec{r}_b).
 \tag{5.1}$$

The  $M_q^{(u)}$  – scheme follows relations (4.1) with the notations:

$$\begin{aligned}
 f_q(\vec{r}_b, t+1) &= M_q^{(u)}(\vec{r}_b, t), \\
 M_q^{(u)}(\vec{r}_b, t) &= R_q^{(u)}(\vec{r}_b, t) + f_q^{p.c. (u)}(\vec{r}_b, t) + w_q^{(u)}(\vec{r}_w, \hat{t}), \quad q \in \Pi^{(u)}, \\
 w_q^{(u)} &= -\alpha^{(u)} j_q^{*b}(\vec{r}_w, \hat{t}), \\
 j_q^{*b}(\vec{r}_w, \hat{t}) &= t_q^* \hat{\rho} u_q^b(\vec{r}_w, \hat{t}),
 \end{aligned}
 \tag{5.2}$$

where  $\hat{\rho}(\vec{r}_w) = \rho_0(\vec{r}_b)$  for the incompressible flow. Otherwise,  $\hat{\rho}(\vec{r}_w)$  can be extrapolated from the bulk or, when  $\vec{r}_w$  lies at a grid node, one can keep

$$\hat{\rho}(\vec{r}_w) = \rho(\vec{r}_b, t+1)$$

as one more unknown variable, equal to the sum of all (known and unknown) populations. This approach has the analogs in [39, 49] for grid boundary points, in [15] for free interface points and in [16] for moving solid/fluid points. We limit ourself mainly

Table 3: The coefficients  $\kappa_0, \kappa_{-1}, \bar{\kappa}_{-1}, \bar{\kappa}_{-2}$ , the corrections  $f_q^{p.c.(u)}$  and the valid range for  $\delta_q$  for the Dirichlet velocity  $M_q^{(u)}$ -schemes. The missing coefficient is  $\kappa_1 = 1 - \kappa_0 - \kappa_{-1} - \bar{\kappa}_{-1} - \bar{\kappa}_{-2}$ .

$M_q^{(u)}$	$\kappa_0$	$\kappa_{-1}$	$\bar{\kappa}_{-1}$	$\bar{\kappa}_{-2}$	$\delta_q$	$f_q^{p.c.(u)}$
BB	0	0	0	0	$\delta_q=1/2$	0
ULI	$1-2\delta_q$	0	0	0	$0 \leq \delta_q \leq 1/2$	0
MGULI						Eq. (5.5)
MULI						Eq. (5.6)
DLI	0	0	$\frac{2\delta_q-1}{2\delta_q}$	0	$1/2 \leq \delta_q$	0
MGDLI						Eq. (5.5)
MDLI						Eq. (5.6)
YLI	$\frac{1-\delta_q}{1+\delta_q}$	0	$\frac{\delta_q}{1+\delta_q}$	0	$0 \leq \delta_q \leq 1$	0
MGYLI						Eq. (5.5)
MYLI						Eq. (5.6)
CLI	$\frac{1-2\delta_q}{1+2\delta_q}$	0	$-\kappa_0$	0	$0 \leq \delta_q \leq 1$	0
MCLI						Eq. (5.6)
MR( $k$ )	$\frac{(\frac{3}{2}-3\delta_q-2\delta_q^2)+2k}{1+k}$	$\frac{(-\frac{1}{2}+\delta_q+\delta_q^2)-k}{1+k}$	$\frac{(\frac{1}{2}-\delta_q)+2k}{1+k}$	$\frac{(-\frac{1}{2}+\delta_q)-k}{1+k}$	$0 \leq \delta_q \leq 1$	Eq. (5.7)
MR1	$\frac{1-2\delta_q-2\delta_q^2}{(1+\delta_q)^2}$	$\frac{\delta_q^2}{(1+\delta_q)^2}$	$-\kappa_0$	$-\kappa_{-1}$		
MGMR(C)	$\frac{1-2\delta_q-2\delta_q^2-4C\Lambda_0}{(1+\delta_q)^2-2C\Lambda_0}$	$\frac{2C\Lambda_0+\delta_q^2}{(1+\delta_q)^2-2C\Lambda_0}$	$\frac{-1+2\delta_q+2\delta_q^2-4C\Lambda_0}{(1+\delta_q)^2-2C\Lambda_0}$	$\frac{2C\Lambda_0-\delta_q^2}{(1+\delta_q)^2-2C\Lambda_0}$		

to incompressible flow below. Table 3 summarizes the principal  $M_q^{(u)}$ -schemes: the bounce-back (BB), the linear interpolations: *upwind/downwind* ULI/DLI from [5] (called also BFL-schemes) and YLI from [46] (which we consider here as a  $M_q^{(u)}$  scheme). We present the *central linear*, three populations based, CLI scheme and show in sequel that CLI, ULI/DLI and YLI belong to the  $LI(\alpha^{(u)})$  family (5.9) which contains an infinite number of second order accurate, “linear” schemes governed by a choice of the coefficient  $\alpha^{(u)}$ . Other new schemes, “linear” MGULI/MGDLI/MGYLI from  $MGLI(\alpha^{(u)})$  sub-family and “parabolic” MULI/MDLI/MYLI and MCLI from  $MLI(\alpha^{(u)})$  family have equal coefficients as ULI/DLI/YLI and CLI, respectively, but differ from them in the correction  $f_q^{p.c.(u)}$ . The  $MGLI(\alpha^{(u)})$  sub-family gets exact parametrization properties for  $LI(\alpha^{(u)})$  family. The  $MLI(\alpha^{(u)})$  family extends its formal accuracy to third-order. Then follows the “parabolic” family MR( $k$ ) from [16], with  $k$  as a free parameter, and its new sub-family MGMR(C), with MR1 = MGMR(C = 0).

We substitute first the coefficients  $\kappa_1 - \bar{\kappa}_{-2}$  into relations (4.8) and (4.9), and specify the coefficients from the Table 2. All schemes yield  $\alpha^{(p)} = 0$  (i.e.,  $A^+ = 1$  and  $D^+ = 1$ ) such that  $\Pi_q, \partial_t \Pi_q$  and  $p_q / \lambda_e$  vanish from the closure relation. The remaining coefficients from the Table 2, *divided by  $\alpha^{(u)}$* , are given in Table 4. The coefficient  $\alpha^{(t)}$  is discussed in Section 5.6.

Table 4: All  $M_q^{(u)}$ -schemes yield  $\alpha^{(p)}=0$ . The table shows the remaining coefficients from Table 2, divided by  $\alpha^{(u)}$ :  $\beta^{(u^*)}=\beta^{(u)}/\alpha^{(u)}$ ,  $\beta^{(p^*)}=\beta^{(p)}/\alpha^{(u)}$ , etc. They define the error  $Err^{(u)}$  in relations (5.3).

$M_q^{(u)}/\alpha^{(u)}$	$\alpha^{(u)}$	$\beta^{(u^*)}$	$\beta^{(p^*)}$	$\beta^{(f^*)}$	$\gamma^{(u^*)}$	$\gamma^{(f^*)}$	$\gamma^{(p^*)}$
BB	2	$\frac{1}{2}$	$-\Lambda_o$	$\Lambda_o$	$-\beta^{(p^*)}\Lambda_e = \Lambda_{eo}$	$\frac{1}{2}\Lambda_o$	$-\frac{1}{2}\Lambda_o$
ULI	2	$\delta_q$	$-\Lambda_o + (\delta_q - \frac{1}{2})$	$\Lambda_o$	$-\beta^{(p^*)}\Lambda_e$	$\delta_q\Lambda_o$	$-\delta_q\Lambda_o$
DLI	$\frac{1}{\delta_q}$	$\delta_q$	$-\Lambda_o + (\frac{1}{2} - \delta_q)$	$\Lambda_o$	$-\beta^{(p^*)}\Lambda_e$	$\delta_q\Lambda_o$	$-\delta_q\Lambda_o$
YLI	$\frac{2}{1+\delta_q}$	$\delta_q$	$-\Lambda_o - \frac{1}{2}$	$\Lambda_o$	$-\beta^{(p^*)}\Lambda_e$	$\delta_q\Lambda_o$	$-\delta_q\Lambda_o$
CLI	$\frac{4}{1+2\delta_q}$	$\delta_q$	$-\Lambda_o$	$\Lambda_o$	$\Lambda_{eo}$	$\delta_q\Lambda_o$	$-\delta_q\Lambda_o$
MR(k)	$\frac{2}{1+k}$	$\delta_q$	$-\Lambda_o$	$\Lambda_o$	$\frac{\delta_q^2}{2} + \Lambda_{eo}$	$\delta_q\Lambda_o$	$-\delta_q\Lambda_o$
MR1	$\frac{4}{(1+\delta_q)^2}$						$+\frac{\delta_q^2-1}{2} + \delta_q - k$
MGMR(C)	$\frac{4}{(1+\delta_q)^2 - 2C\Lambda_o}$						$-\delta_q\Lambda_o$
MGMR2	$\frac{4}{(1+\delta_q)^2 - 2\delta_q\Lambda_o}$						$(C - \delta_q)\Lambda_o$
							0

The MR closure relation takes the form:

$$\begin{aligned}
 \alpha^{(u)} [j_q^* + \delta_q \partial_q j_q^* + \frac{1}{2} \delta_q^2 \partial_q^2 j_q^* + \alpha^{(t)} \partial_t j_q^*] (\vec{r}_b, t) &= \alpha^{(u)} j_q^* (\vec{r}_w, \hat{t}) + (Err^{(u)} - f_q^{p.c. (u)}), \\
 Err^{(u)} &= Err_1^{(u)} + Err_2^{(u)} + Err_3^{(u)}, \\
 Err_1^{(u)} &= \alpha^{(u)} (\delta_q - \beta^{(u^*)}) \partial_q j_q^*, \\
 Err_2^{(u)} &= -\alpha^{(u)} (\beta^{(p^*)} \partial_q \Pi_q^* + \beta^{(f^*)} F_q^* + (\gamma^{(u^*)} - \frac{\delta_q^2}{2}) \partial_q^2 j_q^*), \\
 Err_3^{(u)} &= -\alpha^{(u)} (\gamma^{(f^*)} \partial_q F_q^* + \gamma^{(p^*)} \partial_q^2 \Pi_q^* + \alpha^{(t)} \Lambda_o \partial_t F_q^*).
 \end{aligned}
 \tag{5.3}$$

All  $M_q^{(u)}$  schemes yield

$$\beta^{(u^*)} = \delta_q, \quad Err_1^{(u)} = 0,$$

then they are at least  $j^{(2)}/\Pi^{(1)}$ -accurate (with  $\delta_q = \frac{1}{2}$  for bounce-back). Using the approximation (2.22), one can perform a back substitution for velocity schemes:

$$\partial_q \Pi_q^* = m_q^{(F)} + \Lambda_e \partial_q^2 j_q^* - \partial_t j_q^* + \mathcal{O}(\varepsilon^3), \quad m_q^{(F)} = m_q + S_q^-.
 \tag{5.4}$$

The forcing term then vanishes in  $Err_2^{(u)}$  (i.e.,  $\beta^{(p^*)} m_q^{(F)} + \beta^{(f^*)} F_q^* = \beta^{(p^*)} m_q$ ) when  $S_q^- = F_q^*$  (i.e.,  $\vec{j}^{eq} = \vec{j}$ ) and  $\beta^{(p^*)} = -\beta^{(f^*)}$ . The last condition is verified by BB, CLI/MCLI and

Table 5: The left-hand-side of the approximated steady state MR closure relation. The right-hand-side is equal to  $-w_q^{(u)}/\alpha^{(u)} = j_q^{*b}(\vec{r}_w, \hat{t})$ .

$M_q^{(u)}$	$j_q^*$	$\partial_q j_q^*$	$\partial_q^2 j_q^*$	$F_q^*$	$\partial_q \Pi_q^*$	$\partial_q F_q^* - \partial_q^2 \Pi_q^*$
BB	1	$\frac{1}{2}$	$\Lambda_{e0}$	$\Lambda_o$	$-\Lambda_o$	$\frac{1}{2}\Lambda_o$
ULI/DLI	1	$\delta_q$	$\Lambda_{e0} +  \delta_q - \frac{1}{2} \Lambda_e$	$\Lambda_o$	$-\Lambda_o -  \delta_q - \frac{1}{2} $	$\delta_q \Lambda_o$
YLI	1	$\delta_q$	$\Lambda_{e0} + \frac{\Lambda_e}{2}$	$\Lambda_o$	$-\Lambda_o - \frac{1}{2}$	$\delta_q \Lambda_o$
CLI, MGLI	1	$\delta_q$	$\Lambda_{e0}$	$\Lambda_o$	$-\Lambda_o$	$\delta_q \Lambda_o$
MR1, MCLI	1	$\delta_q$	$\frac{1}{2}\delta_q^2$	0	0	$\delta_q \Lambda_o$
MGMR2	1	$\delta_q$	$\frac{1}{2}\delta_q^2$	0	0	0

MR( $k$ ),  $\forall k$  (see  $\beta^{(f)}, \beta^{(p)}$  in Table 4). We consider the following corrections:

$$f_q^{p.c.(u)} = -\alpha^{(u)}(\beta^{(p*)} + \beta^{(f*)})m_q^{(F)}, \quad \beta^{(f*)} = \Lambda_o, \tag{5.5}$$

$$f_q^{p.c.(u)} = -\alpha^{(u)}[\beta^{(p*)}m_q^{(F)} + \beta^{(f*)}F_q^* + (\gamma^{(u*)} + \Lambda_e\beta^{(p*)} - \frac{\delta_q^2}{2})\partial_q^2 j_q^*], \tag{5.6}$$

$$f_q^{p.c.(u)} = -\alpha^{(u)}(\beta^{(p*)}m_q^{(F)} + \beta^{(f*)}F_q^*). \tag{5.7}$$

The resulting closure relations are given in Table 5. The first correction (5.5) distinguishes the “magic” linear schemes MGLI( $\alpha^{(u)}$ ), e.g., MGULI/MGDLI and MGYLI from ULI/DLI and YLI, respectively. We will show that the MGLI sub-family satisfies the conditions (4.7) and therefore, these schemes support exactly the bulk properties of the solutions with respect to  $\Lambda_{e0}$ . In particular, the permeability of any porous structure computed with these schemes is absolutely viscosity independent when  $\Lambda_{e0}$  is fixed. This property is shared by BB, CLI and MGMR(C) owing to their coefficients. Further details are found in Section 5.2.1. The correction (5.6) removes the second-order error  $Err_2^{(u)}$ : it is used to construct MR( $k$ ) and MLI( $\alpha^{(u)}$ ) families. The terms  $m_q$  and  $S_q^-$  are locally available but  $\partial_q^2 j_q$  needs to be computed unless its coefficient in  $f_q^{p.c.(u)}$  vanishes. The correction (5.6) reduces then to the local relation (5.7) for MR( $k$ ) family.

## 5.2 Space approximation

### 5.2.1 Bounce-back and two-three populations based “linear” schemes,

$$LI(\alpha^{(u)}) = \{CLI, ULI/DLI, YLI, \dots, MGLI(\alpha^{(u)})\}\text{-family}$$

Let the coefficients yield the following conditions (see relations (4.8) and (4.9)):

$$\kappa_{-1} = \bar{\kappa}_{-2} = 0, \quad \alpha^{(p)} = \kappa_1 + \kappa_0 + \bar{\kappa}_{-1} - 1 = 0, \quad \beta^{(u)} = 1 - \kappa_0 = \alpha^{(u)}\delta_q. \tag{5.8}$$

There is then an infinite number of three coefficients  $\{\kappa_0, \bar{\kappa}_{-1}, \kappa_1\}$ , parameterized with free parameter  $\alpha^{(u)} = \kappa_1 + \kappa_0 - \bar{\kappa}_{-1} + 1$ , which satisfy relations (5.8). These three coefficients

build the  $LI(\alpha^{(u)})$  family:

$$\kappa_0 = 1 - \alpha^{(u)}\delta_q, \quad \bar{\kappa}_{-1} = 1 - \frac{\alpha^{(u)}}{2}, \quad \kappa_1 = \alpha^{(u)}\left(\delta_q + \frac{1}{2}\right) - 1. \tag{5.9}$$

The coefficients of the closure relation, divided by  $\alpha^{(u)}$ , are:

$$\begin{aligned} \beta^{(p^*)} &= -\Lambda_o + \left(\frac{1}{2} + \delta_q - \frac{2}{\alpha^{(u)}}\right), & \beta^{(f^*)} &= \Lambda_o, & \gamma^{(u^*)} &= -\beta^{(p^*)}\Lambda_e, \\ \gamma^{(p^*)} &= -\gamma^{(f^*)} = -\delta_q\Lambda_o. \end{aligned} \tag{5.10}$$

The heuristic stability condition  $0 \leq \kappa_1 \leq 1$  is satisfied when

$$\frac{2}{1 + 2\delta_q} \leq \alpha^{(u)} \leq \frac{4}{1 + 2\delta_q}.$$

Two populations schemes ULI (DLI) select the solution with  $\alpha^{(u)} = 2$  ( $\alpha^{(u)} = 1/\delta_q$ , respectively) and their two coefficients lie inside  $[0,1]$ . They reduce to BB for  $\delta_q = \frac{1}{2}$ . An example of a three populations scheme is YLI. This scheme does not reduce to BB for  $\delta_q = \frac{1}{2}$  but it coincides with ULI for  $\delta_q = 0$  and with DLI for  $\delta_q = 1$ .

**Parametrization properties.** The exact steady closure relation reduces to the local, one point form (4.3) for the  $LI(\alpha^{(u)})$  family:

$$[\alpha^{(u)}(j_q^* + \delta_q p_q + \beta^{(p^*)}m_q^{(F)} + \beta^{(f^*)}F_q^*) + f_q^{p.c.(u)}](\vec{r}_b) = \alpha^{(u)}j_q^*(\vec{r}_w). \tag{5.11}$$

The microscopic rule (5.11) obeys the relations (4.7) if

$$\beta^{(p^*)} = \Lambda_o r_i(\Lambda_{eo}, \delta_q, q),$$

where  $r_i$  is either some function of  $\Lambda_{eo}$  or does not depend on the eigenvalues. The bounce-back rule satisfies these properties with  $\beta^{(p^*)} = -\Lambda_o$ . This explains why the components of the permeability tensor  $\mathbf{K}$  are viscosity independent for any porous media when BB is applied and  $\Lambda_{eo}$  is fixed (see the results in [16]).

Neither ULI/DLI nor YLI shares this property, but CLI does: this scheme is fixed by setting

$$\beta^{(p^*)} = -\Lambda_o = -\beta^{(f^*)},$$

in addition to conditions (5.8). Similar to YLI, CLI does not need any switching at  $\delta_q = \frac{1}{2}$  but it reduces to BB for  $\delta_q = \frac{1}{2}$ ; its coefficients  $\kappa_0 = -\bar{\kappa}_{-1}$  are not restricted however to  $[0,1]$  but they lie inside  $[-1,1]$ .

We propose the local correction (5.5) for  $LI(\alpha^{(u)})$  family and call the obtained schemes “magic” linear schemes or MGLI( $\alpha^{(u)}$ ) sub-family. The  $f_q^{p.c.(u)}$  replaces the deficient component,  $\alpha^{(u)}\beta^{(p^*)}m_q^{(F)}$  with the suitable one,  $-\alpha^{(u)}\Lambda_o m_q^{(F)}$ . It is noted that the  $f_q^{p.c.(u)}$  vanishes for CLI. The exact steady closure relation (5.11) are equivalent for the all schemes

from MGLI( $\alpha^{(u)}$ ) family and CLI, although their pre-factors  $\alpha^{(u)}$  differ. The obtained steady solutions are therefore *identical* for MGULI/MGDLI/MGYLI and CLI, but the transient solution, the staggered invariants, the convergence and stability differ. All MGLI( $\alpha^{(u)}$ ) schemes are then controlled with  $\Lambda_{eo}$  for steady solutions and they allow efficient and accurate computations in complex geometries.

**Particular solutions.** For steady or transient, one-dimensional flows invariant along the boundary, the  $Err_2^{(u)}$  can be removed from the closure relation with special solutions for  $\Lambda_{eo}(\delta_q)$ . These solutions are presented in [22] and verified for steady Poiseuille flow and the pulsatile flow [26, 47]. They extend the previous (bounce-back) solution [13, 16] for linear interpolations and for an arbitrary distance,  $0 \leq \delta_q \leq 1$ . The CLI and all MGLI( $\alpha^{(u)}$ ) schemes yield an exact prescribed location of the solid walls in parabolic flow when

$$\Lambda_{eo} = \frac{3\delta_q^2}{4}, \quad \delta_q \geq 0. \tag{5.12}$$

When  $\delta_q^2 = \frac{1}{2}$  the solution reduces to  $\Lambda_{eo} = \frac{3}{16}$ , previously obtained in [13, 16] for BB. When  $\delta_q = 0$ , then  $\Lambda_o = 0$ , a stability limit of the model.

Alternative solution [22] redefines  $\delta_q$  for the coefficients of the linear schemes such that Poiseuille flow in arbitrary inclined channel is modeled exactly. The coefficients depend then, however, on  $\Lambda_{eo}$  and the assumed channel width.

**5.2.2 Two-three populations based “parabolic” schemes,**

**MLI( $\alpha^{(u)}$ ) = {MCLI, MULI/MDLI, MYLI, ...}-family**

The LI( $\alpha^{(u)}$ ) family is robust but exact in general only for linear velocity and constant pressure solutions. The idea of the (*modified*) MLI( $\alpha^{(u)}$ ) family is to remove  $Err_2^{(u)}$  with  $f_q^{p.c.(u)}$  (relation (5.6)), without altering the coefficients, but involving a finite-difference (f.d) approximation for  $\partial_q^2 j_q^*$ . It is noted that  $\gamma^{(u^*)} = -\Lambda_e \beta^{(p^*)}$  for LI( $\alpha^{(u)}$ ) family (cf. relations (5.10)), then  $f_q^{p.c.(u)}$  correction (5.6) becomes for MLI:

$$f_q^{p.c.(u)} = -\alpha^{(u)} \left( \beta^{(p^*)} m_q^{(F)} + \beta^{(f^*)} F_q^* - \frac{\delta_q^2}{2} \partial_q^2 j_q^* \right). \tag{5.13}$$

One needs to approximate  $\partial_q^2 j_q^*$  when  $\delta_q \neq 0$ , e.g. with the help of a link-wise f.d. approximation:

$$\partial_q^{2f.d} j_q^* \approx \frac{2}{\delta_q + \delta_{\bar{q}}} \left( \frac{j_q^*(\vec{r}_w, \hat{t}) - j_q^*(\vec{r}_b, \hat{t})}{\delta_q} - \frac{j_q^*(\vec{r}_b, \hat{t}) - j_q^*(\vec{r}_{\bar{w}}, \hat{t})}{\delta_{\bar{q}}} \right) + \mathcal{O}(\varepsilon^3), \tag{5.14}$$

where

$$\vec{r}_w = \vec{r}_b + \delta_q \vec{c}_q, \quad \vec{r}_{\bar{w}} = \vec{r}_b + \delta_{\bar{q}} \vec{c}_{\bar{q}}, \quad \delta_q \neq 0, \quad \delta_{\bar{q}} \neq 0.$$

Here,  $j_q^*(\vec{r}_w, \hat{t})$  is computed with a prescribed Dirichlet value. The solution in the neighboring grid point,  $j_q(\vec{r}_b - \vec{c}_q, \hat{t})$ ,  $\delta_q = 1$ , is either already updated,  $\hat{t} = t + 1$ , or taken from the previous time step,  $\hat{t} = t$ , or combined. We discuss in section 5.2.4 how the MLI family may maintain the third accuracy in corners. On the whole we find that the stability of MLI and MGLI schemes is very similar. The solutions with MULI/MDLI and MCLI (which are equal at steady state) are quite comparable with MGMR(C) solutions, although MR1 gains more often in accuracy for steady and temporal flow. We observe that in closed rectangular boxes, the most robust is a combination of MLI and MR1 for two adjacent boundaries.

**Parametrization properties.** The MLI family completely removes the term associated with  $m_q^{(F)}$  and  $F_q^*$  from the closure relation (5.11). It is understood that if the discretized velocity distribution obeys some parametrization properties, so does any finite-difference combination of velocity values. The MLI family satisfies therefore the conditions (4.7) and its steady solutions are fully controlled by the non-dimensional hydrodynamic numbers and  $\Lambda_{e0}$ .

### 5.2.3 Five populations based “parabolic” schemes: MR( $k$ )-family

This family cancels the coefficients in front of  $\partial_q^2 j_q^*$  in the  $f_q^{\text{p.c.}(u)}$  correction (5.6) with the help of the five coefficients  $\kappa_1 - \bar{\kappa}_{-2}$ . They satisfy the linear system of equations:

$$\begin{aligned} \alpha^{(p)} &= A^+ - 1 = 0, & \beta^{(u)} &= A^+ + B^- = \alpha^{(u)} \delta_q, \\ A^+ + A^- + 1 &= \alpha^{(u)} = \frac{2}{k+1}, & & \\ \gamma^{(u)} + \Lambda_e \beta^{(p)} &= \frac{\alpha^{(u)}}{2} \delta_q^2, & \beta^{(p)} &= -\beta^{(f)} = -\alpha^{(u)} \Lambda_o. \end{aligned} \quad (5.15)$$

The free parameter  $\alpha^{(u)}$  is parameterized with  $k$ , following the original work [16]. The  $f_q^{\text{p.c.}(u)}$  reduces to relation (5.7):

$$f_q^{\text{p.c.}(u)} = \text{Err}_2^{(u)} = \alpha^{(u)} \Lambda_o (m_q^{(F)} - F_q^*). \quad (5.16)$$

This term is equal to  $\alpha^{(u)} \Lambda_o m_q$  when  $\vec{j}^{\text{eq}} = \vec{J}$ ,  $S_q^- = F_q^*$  (this set-up is used in [16]). The MR( $k$ ) yields the triplet  $j^{(3)}/\Pi^{(2)}/F^{(1)}$  for all  $k$ . The optimal solutions for  $k$ , based on heuristic stability arguments, i.e.,

$$\kappa_1 = \frac{2\delta_q + \delta_q^2 - k}{1+k} \in [0;1], \quad \{\kappa_0, \bar{\kappa}_{-1}, \kappa_{-1}, \bar{\kappa}_{-2}\} \in [-1;1],$$

are given in [16]. The last condition (5.15),  $\beta^{(p)} = -\alpha^{(u)} \Lambda_o$ , is not necessary to reach the prescribed accuracy but appears to be very helpful for the parametrization properties. Below we discuss the MR1 scheme and the MGMR(C) sub-family. Both yield an exact parametrization owing to special solutions for  $k$ .

**Parametrization properties and MR1 scheme.** It was discovered that a particular MR( $k$ ) scheme

$$\text{MR1: } k = k(\delta_q) = \frac{1}{2}(1 + \delta_q)^2 - 1, \quad \text{then } \kappa_1 = 1, \quad (5.17)$$

yields permeability values absolutely independent of the viscosity (see Table III in [16]). The MR1 coefficients lie inside the interval  $[-1, 1]$  but represent the limit of “optimal” solutions for  $\kappa_1$ . The following conditions are sufficient to satisfy relations (4.7):

$$\begin{aligned} \kappa_1 + \kappa_0 + \bar{\kappa}_{-1} - 1 &= 0, & \kappa_{-1} + \bar{\kappa}_{-2} &= 0, \\ (\kappa_1 - \bar{\kappa}_{-1}) &= \frac{1}{2}(\kappa_1 - \bar{\kappa}_{-1} + \kappa_0 + 1), & \bar{\kappa}_{-2} &= \frac{\bar{\kappa}_{-2} - \kappa_{-1}}{2}. \end{aligned} \quad (5.18)$$

The first condition guarantees that  $A^{(p)}(\vec{r})$  and  $A^{(p)}(\vec{r}_b - \vec{c}_q)$  vanish from the closure relation for both points. The second condition guarantees that  $B^{(p)}$  is proportional to  $\Lambda_o$  for them. The solution to relations (5.18) is:

$$\kappa_1 = 1, \quad \kappa_0 = -\bar{\kappa}_{-1}, \quad \kappa_{-1} = -\bar{\kappa}_{-2}. \quad (5.19)$$

When  $\kappa_1 = 1$ , then  $k = k(\delta_q)$ . This particular choice results in the MR1 scheme which satisfies relations (5.19) and relations (4.7). If we set  $\kappa_{-1} = \bar{\kappa}_{-2} = 0$ ,  $f_q^{\text{p.c.}} = 0$  and the solution (5.19) is the CLI scheme.

**Parametrization properties and MGMR(C) sub-family.** Let the local solution components be labeled with “loc” and those in  $\vec{r}_b - \vec{c}_q$  with “nb”. The exact steady closure relation (4.5) with (4.6), divided by  $\alpha^{(u)}$ , becomes then for the MR( $k$ )–family (including correction  $f_q^{\text{p.c.}(u)}$ ):

$$\begin{aligned} j_q^{\star \text{loc}} + \delta_q p_q^{\text{loc}} + A^{(u) \text{nb}}(j_q^{\star \text{nb}} - j_q^{\star \text{loc}} + p_q^{\text{loc}}) + B^{(u) \text{nb}}(p_q^{\text{nb}} - p_q^{\text{loc}}) \\ + A^{(p) \text{nb}}(\Pi_q^{\star \text{nb}} - \Pi_q^{\star \text{loc}} + m_q^{(F) \text{loc}}) + B^{(p) \text{nb}}(m_q^{(F) \text{nb}} - m_q^{(F) \text{loc}}) \\ + A^{(u) \text{nb}} \Lambda_o (F_q^{\star \text{nb}} - F_q^{\text{loc}}) = j_q^{\star b}, \end{aligned} \quad (5.20)$$

where

$$\begin{aligned} A^{(p) \text{nb}} &= \frac{\kappa_{-1} + \bar{\kappa}_{-2}}{\alpha^{(u)}} = \frac{(1 + \delta_q)^2}{2} - 1 - k, & A^{(u) \text{nb}} &= \frac{\delta_q^2}{2}, \\ B^{(u) \text{nb}} &= -\frac{\delta_q^2}{4} - \Lambda_e A^{(p) \text{nb}}, & B^{(p) \text{nb}} &= -\Lambda_o \frac{\delta_q^2}{2} - \frac{A^{(p) \text{nb}}}{2}. \end{aligned} \quad (5.21)$$

The MR1 solution yields  $A^{(p) \text{nb}} = 0$  and all coefficients (5.21) satisfy the sufficient conditions (4.7), in agreement with the analysis above. Another possible solution is to set

$A^{(p)nb} = C\Lambda_o$ , then all coefficients in relation (5.20) satisfy the conditions (4.7). This results in sub-family MGMR(C),

$$\text{MGMR}(C): k = k(C) = k(\delta_q) - C\Lambda_o, \quad C^{min} \leq C\Lambda_o \leq 0. \quad (5.22)$$

In principle,  $C$  may represent a constant or a function of  $\delta_q$  and/or  $\Lambda_{eo}$ . The stability bounds yield

$$\kappa_1 = \frac{(1+\delta_q)^2 + 2C\Lambda_o}{(1+\delta_q)^2 - 2C\Lambda_o} \in [0, 1]$$

and all other coefficients inside  $[-1, 1]$  when

$$C^{min} = \begin{cases} -2\delta_q - \frac{3}{2}\delta_q^2 & \text{for } 0 \leq \delta_q \leq \delta_0 \ (\kappa_0 = 1), \\ \frac{\delta_q^2}{2} - 1 & \text{for } \delta_0 \leq \delta_q \leq 1 \ (\bar{\kappa}_{-1} = 1), \end{cases}$$

where  $\delta_0 = \frac{\sqrt{3}-1}{2}$ . MGMR(C) may show superior stability properties in comparison with MR1: MR1 presents the limit of MGMR(C) when  $C \rightarrow 0$ , e.g. when  $\delta_q \rightarrow 0$  or  $\Lambda_o \rightarrow \infty$ . The MGMR(C) sub-family guaranties equal steady solutions on a given grid when the hydrodynamic numbers and  $\Lambda_{eo}$  are fixed provided that  $C$  takes the same value, e.g., if

$$0 \leq \Lambda_o = \frac{\Lambda_{eo}}{\Lambda_e} \leq \Lambda_o^{max},$$

then

$$\frac{C^{min}}{\Lambda_o^{max}} \leq C \leq 0.$$

The MGMR(C) family cancels the  $\gamma^{(p)}\partial_q^2\Pi_q^*$  term in the closure relation when  $C = \delta_q$ :

$$\text{MGMR2}: k = k(C) = k(\delta_q) - \delta_q\Lambda_o. \quad (5.23)$$

The MGMR2 yields then the triplet  $j^{(3)}/\Pi^{(3)}/F^{(1)}$ , i.e., it is exact for parabolic velocity and pressure distributions. However, its coefficient  $\kappa_1$  exceeds 1 ( $C > 0$  when  $\delta_q > 0$ ) and it remains stable only when the free parameter  $\Lambda_o$  is very small (typically,  $\Lambda_o \approx 10^{-2}$ ). The MGMR2 is then too restrictive for general modeling, but allows to verify the third-order expansion and boundary analysis. As an example, the MGMR2 is exact for the parabolic pressure and linear velocity solutions [33] for the incompressible Navier-Stokes equations, with and without forcing. We discuss these solutions in [22].

#### 5.2.4 Special links with $M_q^{(u)}$

For the first-type links, we restrict the five population schemes to the two-point form (4.2). One can also switch to the MLI( $\alpha^{(u)}$ ) family. For the second type of special links, the schemes from MLI-family are applied in a "local" form (4.3). When

$$\vec{r}_w = \vec{r}_b + \delta_{\vec{q}}\vec{c}_{\vec{q}} \in \Gamma^{(u)},$$

one can still apply them with the relations (5.14). For each of the two opposite velocities, the exact steady closure relation is given by relation (5.11). When  $\delta_q > 0$ ,  $\delta_{\bar{q}} > 0$  and  $\delta_q \neq \delta_{\bar{q}}$ , the two conditions are independent and non-trivial. When two links have equal coefficients (e.g.,  $\delta_q = \delta_{\bar{q}}$ ) and  $f_q^{\text{p.c.}(u)} = -f_{\bar{q}}^{\text{p.c.}(u)}$ , the sum and the difference of relation (5.11) give two conditions:

$$\beta^{(u)} p_q(\vec{r}_b) = \alpha^{(u)} t_q^* (j_q^b(\vec{r}_w) - j_q^b(\vec{r}_{\bar{w}})), \quad (5.24)$$

$$[\beta^{(f)} F_q^* + \beta_q^{(p)} m_q^{(F)} + f_q^{\text{p.c.}(u)}](\vec{r}_b) = \alpha^{(u)} \frac{\delta_q^2 j_q^{*b}(\vec{r}_w) - 2j_q^*(\vec{r}_b) + j_q^{*b}(\vec{r}_{\bar{w}})}{2\delta_q^2}. \quad (5.25)$$

The LI and MLI families yield  $\beta^{(u)} = \alpha^{(u)} \delta_q$  such that the first condition constrains  $p_q(\vec{r}_b)$  to its directional central approximation. The second constraint vanishes for the MLI family if  $f_q^{\text{p.c.}(u)}$  is computed with relation (5.6) using relations (5.14). Then the obtained solution loses its uniqueness. We recommend to use (for second-type links only) a  $m_q^{(F)}$ -based approximation instead of relations (5.14):

$$\begin{aligned} \partial_q^2 j_q^*(\vec{r}_b, t) &\approx -\frac{m_q^{(F)} - \partial_q^{f.d} \Pi_q^*}{\Lambda_e}, & \partial_q^{f.d} \Pi_q^* &= -\sum_{\alpha=1}^d \partial_\alpha^{f.d} \Pi_q^* c_{\bar{q}\alpha}, \\ \partial_\alpha^{f.d} \Pi_q^* c_{\bar{q}\alpha} &= \Pi_q^*(\vec{r}_b + c_{\bar{q}\alpha}) - \Pi_q^*(\vec{r}_b). \end{aligned} \quad (5.26)$$

We assume here that the  $c_{\bar{q}\alpha}$  are parallel to the principal coordinate axis. A sub-set of the next grid neighbors  $\{\vec{r}_b + c_{\bar{q}\alpha}\}$  is available, except perhaps for some specific “sharp corner” discretization.

### 5.3 Numerical example

Several Stokes and Navier-Stokes flows around cubic arrays of spheres, square array of cylinders, reconstructed fiber materials and moving solids in [16], using the  $d3Q15$  velocity set, and with body-centered cubic arrays of spheres and a random-size sphere-packed porous medium in [40], using  $d3Q19$  velocity set, have validated the multi-reflection approach for arbitrary shaped, relatively smooth boundaries. They have confirmed the high accuracy of the  $\text{MR}(k)$  family in the context of moderate resolutions. Using the BB and MR1, the permeability (3.10) of any porous structure is viscosity independent when the free eigenvalue function  $\Lambda_o$  varies together with  $\Lambda_e$  such that  $\Lambda_{eo} = \Lambda_e \Lambda_o$  keeps a constant value. These numerical results have been formally obtained with MRT models but in their reduced, TRT version (see also in Section 8).

Let us here give only one example. We consider again a Stokes flow around a cubic array of spheres and use the  $d3Q15$  velocity set. For the two most dense arrays *the first-type links* appear. For them we switch MR1 to the two points form (4.2). The relative error

$$E^{(r)}(k) = k/k^{ref} - 1$$

Table 6: Comparison of the relative permeability errors  $E^{(r)}(k)[\%]$  for a cubic array of spheres in a  $25^3$  box using several link-wise boundary schemes. The error is controlled by  $\Lambda_{eo}$  for BB, CLI, MR1 and MCLI. The steady solutions are identical for all MLI( $\alpha^{(u)}$ ) schemes (MCLI here) and for CLI and all MGLI( $\alpha^{(u)}$ ) schemes, respectively.

$\chi$	$\Lambda_{eo} = \frac{3}{16}$				$\Lambda_{eo} = \frac{1}{4}$				$\Lambda_{eo} = \frac{3}{4}$			
	BB	CLI	MR1	MCLI	BB	CLI	MR1	MCLI	BB	CLI	MR1	MCLI
0.5	-1.0	0.57	-0.42	$-6.6 \times 10^{-2}$	0.16	1.55	-0.14	0.29	7.2	8.0	1.8	2.7
0.6	-3.0	0.05	-0.46	-0.12	1.83	0.95	-0.22	0.20	4.9	6.9	1.5	2.4
0.7	-2.1	0.10	-0.44	-0.12	0.87	1.03	-0.23	0.17	6.4	7.2	1.3	2.1
0.85	-1.5	1.1	-0.35	$-4 \times 10^{-4}$	3.2	2.4	-0.23	0.22	13	11	0.6	1.6
0.90	-4.4	-0.05	-0.67	-0.16	2.59	1.4	-0.5	0.1	8.0	10.1	0.16	1.6
0.95	-4.3	0.28	-0.56	0.05	2.28	2.0	-0.46	0.34	9.7	13	0.22	2.2

is computed with respect to the reference permeability value  $k^{ref}$ , based on the quasi-analytical solution for the drag force on a sphere given in [1, 25, 42]. Exact formulas, the tabulated values we are using and the numerical parameters can be found in [16].

We confirm that the *macroscopic solutions and permeability values are identical* and controlled by  $\Lambda_{eo}$  for CLI and MGLI( $\alpha^{(u)}$ ), e.g. MGULI/MGDLI and MGYLI. The solutions are also controlled by  $\Lambda_{eo}$  for MLI( $\alpha^{(u)}$ ) and MGMR(C) families (with MR1 as a particular element). We start from a uniform density and zero velocity equilibrium distribution. The convergence to steady state differs, because the coefficients are different, but the number of steps has typically the same order of magnitude within one family when the viscosity and  $\Lambda_{eo}$  are fixed. Higher  $\Lambda_{eo}$  values may accelerate the convergence at fixed viscosity. At the same time, the errors generally increase with  $\Lambda_{eo}$ , owing to the increase of the coefficients in front of the higher-order derivatives in the bulk and boundary macroscopic relations. The relative errors in permeability in Table 6 are given for  $\Lambda_{eo} = \{\frac{3}{16}, \frac{1}{4}, \frac{3}{4}\}$ , versus relative solid concentration values  $\chi = c/c^{max}$ ,  $c^{max} = \pi/6$ . It is noted that  $\Lambda_{eo} = \frac{3}{16}$  ( $\frac{3}{4}$ ) yields for MGLI the exact parabolic flow in a straight channel with a distance  $\delta_q = \frac{1}{2}$  (respectively,  $\delta_q = 1$ ) to boundaries. We keep then  $\Lambda_{eo} = \frac{3}{4}$  as a reasonable upper accuracy limit. The results with BB and MR1 for  $\Lambda_{eo} = \frac{3}{16}$  are the same as in [16] (Table IV therein).

The accuracy of the “magic” linear schemes (see CLI in Tables 6 and 7) clearly surpasses the bounce-back rule for  $\Lambda_{eo} = \frac{3}{16}$  but is similar to it for  $\Lambda_{eo} = \frac{3}{4}$ . This indicates once more the role of  $\Lambda_{eo}$  on the actual second-order error. There is no solution for  $\Lambda_{eo}$  which gives the best accuracy for the any geometry. It often happens that the error goes through zero when  $\Lambda_{eo}$  varies inside the interval  $[0, 1]$  (here, inside  $[\frac{3}{16}, \frac{1}{4}]$  for MCLI and  $[\frac{1}{4}, \frac{3}{4}]$  for MR1), resulting in a very high precision for particular  $\Lambda_{eo}$  values. One should keep  $\Lambda_{eo}$ , roughly speaking, below  $\frac{3}{4}$  for linear schemes and not much higher than 1 for parabolic schemes. Related to truncated terms, e.g.,  $\gamma^{(p)} \partial_q^2 \Pi_q^*$ , the difference between the results obtained with MR1 and MGMR(C) depends on a selected value C, and converges

Table 7: Comparison of the relative permeability errors  $E^{(r)}(k)[\%]$  for a cubic array of spheres in a  $25^3$  box using linear schemes when  $\Lambda_{eo}=3/16$ . The permeability is independent of the viscosity  $\nu$  only for CLI when  $\Lambda_{eo}$  is fixed.

$\chi$	$\forall \nu$	$\nu = \frac{1}{30}$		$\nu = \frac{1}{6}$		$\nu = \frac{1}{2}$		$\nu = \frac{3}{2}$	
		CLI	ULI/DLI	YLI	ULI/DLI	YLI	ULI/DLI	YLI	ULI/DLI
0.5	0.57	0.9	1.2	2	3.5	4.3	8.0	8.8	16
0.6	0.05	0.3	0.6	1.3	2.8	3.3	7.1	7.8	16
0.7	0.1	0.4	0.8	1.4	3.2	3.6	8.1	8.4	18
0.85	1.1	1.7	2.3	3.6	6.6	7.7	15.5	17	34
0.95	0.28	1.0	1.9	4.0	8.1	10.3	21.3	24.2	50.4

to zero when  $C \rightarrow 0$ . We detect usually that MR1 results are slightly more accurate.

In Stokes flow modeled with ULI/DLI and YLI, the second-order boundary error, with respect to the viscosity independent solution  $\vec{v}_j^*$ , varies as  $|\delta_q - \frac{1}{2}| \Lambda_e^2$  and  $\frac{1}{2} \Lambda_e^2$ , respectively (see the coefficients in front of  $\partial_q^2 j_q^*$  in Table 5). One should expect then the increase of errors in permeability measurements with  $\Lambda_e$ , even when  $\Lambda_{eo}$  is fixed. It is noted that for YLI this error does not vanish when  $\delta_q = \frac{1}{2}$ . The results in Table 7 are computed with ULI/DLI and YLI (they coincide for ULI/DLI with those in Table V in [16] when  $\nu = \frac{1}{30}$  ( $\tau = 0.6$  there) and  $\nu = \frac{1}{2}$ ). The results with CLI are those from the previous table. We observe that CLI overtakes ULI/DLI in accuracy even for relatively small viscosity. In its turn, ULI/DLI surpasses YLI by a factor 2 for all tests. Although the situation may in principle become inverse, for other  $\Lambda_{eo}$  value and/or smaller viscosities, we return to this conclusion systematically. Finally, the errors increase rapidly with the viscosity and they reach, roughly, those of bounce-back (see in previous table) already for  $\nu = \frac{1}{6}$ . Although one could advocate the use of small viscosity values ( $\lambda_e < -1$ ), we emphasize that the convergence time increases as the inverse of  $\nu$ , even when  $\Lambda_{eo}$  is fixed. In case of the BGK,  $\Lambda_{eo}$  behaves as  $\nu^2$  and requires the use of even smaller viscosities. Also, it is not possible to keep small values for two viscosities, e.g., for two phase simulations with high viscosity ratio.

## 5.4 Staggered invariants

Spurious conserved quantities have already been known for Lattice Gas modeling and have been discussed by Zanetti in [48].

### 5.4.1 One particular staggered solution

We will refer here to “staggered solution” as a one dimensional velocity component  $u_y(y, t)$  which oscillates between two time measurements in a periodic channel composed

of  $N_y$  horizontal lines (numbered with superscript):

$$\begin{aligned} u_y^{(2l)}(t) &= (-1)^{t+1} u^s, \quad l=1,2,\dots,N_y/2, \\ u_y^{(2l-1)}(t) &= (-1)^t u^s, \quad l=1,2,\dots,(N_y+1)/2, \quad t=0,1,2,\dots \end{aligned} \quad (5.27)$$

Substituting the equilibrium distribution with the staggered solution (5.27) (and  $p_q=0$ ,  $m_q^{(F)}=0$ ,  $F_q^*=0$ ) into the exact closure relation, one finds that  $M_q^{(u)}$ -scheme supports it if, necessarily:

$$(\kappa_1 - \kappa_0 - \bar{\kappa}_{-1} + \kappa_{-1} + \bar{\kappa}_{-2}) u^s = u^s. \quad (5.28)$$

Since

$$A^+ = \kappa_1 + \kappa_0 + \bar{\kappa}_{-1} + \kappa_{-1} + \bar{\kappa}_{-2} = 1$$

for all  $M_q^{(u)}$  schemes, then the necessary conditions are:

$$\kappa_0 + \bar{\kappa}_{-1} = 0, \quad \kappa_1 + \kappa_{-1} + \bar{\kappa}_{-2} = 1. \quad (5.29)$$

These conditions are met by BB, CLI/MCLI and MR1. The  $f_q^{\text{p.c.}(u)}$  correction (5.7) vanishes for MR1 on the solution (5.27), the BB, CLI and MR1 schemes support then the staggered solution exactly. The  $f_q^{\text{p.c.}(u)}$  reduces to  $\alpha^{(u)} \frac{\delta_q^2}{2} \partial_q^2 j_q^*$  for MCLI, and it differs from zero for the solution (5.27) unless  $\delta_q=0$ .

A simple initialization of the staggered solution (5.27) in an open channel with the no-slip horizontal walls confirms that it is kept by the BB, CLI and MR1 but it is damped for MCLI (except when  $\delta_q=0$ ). The oscillating vertical velocity can coexist with the physical solution of a problem, e.g. the channel flow invariant along its direction. A simple method to kill it is to use the "delayed" value  $\tilde{f}_q(\vec{r}_b, t-1)$  of the outgoing population. The "delayed" bounce-back is therefore:

$$f_{\bar{q}}(\vec{r}_b, t+1) = \tilde{f}_q(\vec{r}_b, t-1). \quad (5.30)$$

The use of the "delayed" values can worsen, however, the conservation and stability properties of the scheme. We mention that the oscillations in time are not restricted to one dimension in space in closed boxes. Their development is related to the existence of staggered invariants supported by the boundary conditions.

#### 5.4.2 Staggered invariants of the BB, CLI and MR1 schemes

The staggered invariant obeys the relation

$$S(t) = -S(t+1) \quad \text{then} \quad S(t) + S(t+1) = 0, \quad \forall t. \quad (5.31)$$

In an open channel consisting of  $N_\perp$  lines parallel to the solid walls, the following combinations of the perpendicular momentum values  $\vec{J}_n(\vec{r}, t)$  satisfy this relation for BB, CLI

and MR1:

$$\begin{aligned}
 N_{\perp} = 2K + 1: \\
 S(t) &= \left( \sum_{l=1}^K \bar{J}_n^{(2l)} - \sum_{l=1}^{K+1} \bar{J}_n^{(2l-1)} \right) - \kappa_0 \left( \sum_{l=1}^K \bar{J}_n^{(2l)} - \sum_{l=2}^K \bar{J}_n^{(2l-1)} \right) \\
 &\quad + \kappa_{-1} \left( \sum_{l=2}^{K-1} \bar{J}_n^{(2l)} - \sum_{l=2}^K \bar{J}_n^{(2l-1)} \right), \\
 N_{\perp} = 2K: \\
 S(t) &= \left( \sum_{l=1}^K \bar{J}_n^{(2l)} - \sum_{l=1}^K \bar{J}_n^{(2l-1)} \right) - \kappa_0 \left( \sum_{l=1}^{K-1} \bar{J}_n^{(2l)} - \sum_{l=2}^K \bar{J}_n^{(2l-1)} \right) \\
 &\quad + \kappa_{-1} \left( \sum_{l=2}^{K-1} \bar{J}_n^{(2l)} - \sum_{l=2}^{K-1} \bar{J}_n^{(2l-1)} \right).
 \end{aligned} \tag{5.32}$$

Owing to the momentum conservation by the collision operator, the total normal momentum is exchanged (no forcing) for even and odd numbered lines, excepted at the boundary lines. Relations (5.32) are derived by replacing the incoming populations with their actual solutions. They combine the difference in total perpendicular momentum for even and odd numbered lines in the initial column (first term in the *RHS*, for BB, CLI and MR1), in the column reduced by two boundary lines (second term in the *RHS*, for CLI and MR1), and finally, in a one reduced by two lines near each boundary (last term in the *RHS*, for MR1). The following relations illustrate a derivation of this solution for CLI scheme ( $\kappa_1 = 1, \kappa_0 = -\bar{\kappa}_{-1}$ ) when  $N_{\perp} = 2K + 1$ , then:

$$\begin{aligned}
 \left( \sum_{l=1}^K \bar{J}_n^{(2l)} - \sum_{l=1}^{K+1} \bar{J}_n^{(2l-1)} \right) (t+1) &= \left( \sum_{l=1}^{K+1} \bar{J}_n^{(2l-1)} - \sum_{l=1}^K \bar{J}_n^{(2l)} \right) (t) + \kappa_0 \vec{\Delta}^b(t), \\
 \left( \sum_{l=1}^K \bar{J}_n^{(2l)} - \sum_{l=2}^K \bar{J}_n^{(2l-1)} \right) (t+1) &= \left( \sum_{l=2}^K \bar{J}_n^{(2l-1)} - \sum_{l=1}^K \bar{J}_n^{(2l)} \right) (t) + \vec{\Delta}^b(t), \\
 \vec{\Delta}^b(t) &= \left( \sum_{q \in \Pi^{(u)}} \tilde{f}_q^{(2K)}(t) \vec{c}_{qn} + \sum_{q \in \Pi^{(u)}} \tilde{f}_q^{(2K+1)}(t) \vec{c}_{\bar{q}n} \right) + \left( \sum_{q \in \Pi^{(u)}} \tilde{f}_q^{(2)}(t) \vec{c}_{qn} + \sum_{q \in \Pi^{(u)}} \tilde{f}_q^{(1)}(t) \vec{c}_{\bar{q}n} \right).
 \end{aligned} \tag{5.33}$$

Combining these relations, one gets relation (5.31) with  $S(t)$  given by the first relation (5.32) when  $\kappa_{-1} = 0$ . For the bounce-back ( $\kappa_0 = 0, \kappa_{-1} = 0$ ), the staggered invariant represents the difference of the total normal momentum for even and odd numbered lines. One can trigger the staggered vertical velocity (5.29) initializing its uniformly,  $u_y(t=0) = u^0$ , in open channel when  $N_y = N_{\perp}$  is odd. Substituting  $J_n(t=0) = u^0$  into relation (5.32), one gets the solution for the staggered amplitude  $|u^s|$ :

$$N_{\perp} = 2K + 1: |u^s| = \frac{(1 + \kappa_0 + \kappa_{-1})|u^0|}{N_{\perp} - (N_{\perp} - 2)\kappa_0 + (N_{\perp} - 4)\kappa_{-1}}. \tag{5.34}$$

For the bounce-back, the initial value is equally distributed over all nodes:  $|u^s| = |u^0|/N_\perp$ . When  $\delta_q = 0$ , the coefficients coincide for CLI, MCLI and MR1 ( $\kappa_1 = \kappa_0 = -\bar{\kappa}_{-1} = 1$ ,  $\kappa_{-1} = \bar{\kappa}_{-2} = 0$ ) and all of them converge to the solution (5.34) where the amplitude is equal to its initial value,  $|u^s| \equiv |u^0|$ . When the number of the grid lines parallel to the solid wall is even,  $N_\perp = 2K$ , the staggered invariant (5.32) vanishes on the uniform initial distribution  $u_y(t=0) = u^0$ . One can provoke the solution (5.27) initializing  $u_y = u^0$  for one row, say the last one. Then

$$|u^s| = \frac{|u^0|}{N_\perp - (N_\perp - 2)\kappa_0 + (N_\perp - 4)\kappa_{-1}},$$

and, again,  $|u^s| = |u^0|/N_\perp$  for the bounce-back. In closed boxes the staggered invariants exist but in a more complicated form.

### 5.5 About the uniqueness of the steady solutions

Starting from different (arbitrary) initial distributions, one could expect to obtain equal steady macroscopic and population solutions. We distinguish three contrary situations.

The first one is when the obtained solution is not steady but oscillates for each two (or more) time moments. The boundary schemes which do not maintain the simple staggered solution (5.27), e.g., the LI schemes (excepted BB and CLI) and the parabolic ones (excepted MR1 and MCLI ( $\delta_q = 0$ )), usually do not show the appearance of oscillating solutions in closed rectangular boxes. One can try to avoid their development with the help of an accurate initialization, e.g. [38], or removing at  $t=0$  the open channel staggered invariants (5.32), at least.

The second situation happens when the solution for second-type link is decoupled from the evolution of the whole system. Indeed, the case  $\delta_q = \delta_{\bar{q}} = 0$  is degenerated for the link-wise approach since two anti-parallel links cut the wall at the same point (see in Fig. 3). One example gives then the ULI scheme. Applied in a local form (4.3) for such a link, its solution is:

$$f_{\bar{q}}(\vec{r}_b, t+1) = f_q(\vec{r}_b, t) - 2j_q^{*b}(\hat{t}), \quad f_q(\vec{r}_b, t+1) = f_{\bar{q}}(\vec{r}_b, t) + 2j_{\bar{q}}^{*b}(\hat{t}).$$

These two anti-parallel populations are decoupled from the others (their initial values are exchanged for no-slip condition). The local MGULI scheme,

$$\begin{aligned} f_{\bar{q}}(\vec{r}_b, t+1) &= f_q(\vec{r}_b, t) - 2j_q^{*b}(\hat{t}) + m_q^{(F)}(t), \\ f_q(\vec{r}_b, t+1) &= f_{\bar{q}}(\vec{r}_b, t) + 2j_{\bar{q}}^{*b}(\hat{t}) - m_q^{(F)}(t), \end{aligned}$$

ouples the second-type link with the other corner populations via  $m_q^{(F)}(t)$  (note that the sum of two solutions remains equal to its initial value). We recommend to use MGULI for the second-type links in solid grid vertexes, bearing also in mind that it yields the correct parametrization properties, or to avoid the solid vertexes on the discretization grid.

The third situation is when the number of the non-trivial independent boundary constraints is less than a number of the unknown population components. Let us consider the “parabolic” schemes in a standard node when  $\delta_q = 0$  ( $\vec{r}_b = \vec{r}_w$ ). The MCLI and MR1 coincide then (MGMR(C) reduces to MR1) and  $\kappa_0 = 1$ ,  $\kappa_1 = \bar{\kappa}_{-1} = 0$  for MULI=MYLI, two other coefficients vanish for all schemes. Replacing  $f_{\bar{q}}(t+1)$  with its boundary solution, e.g.,

$$f_{\bar{q}}(t+1) = f_q(t+1) + f_q^{\text{p.c.}(u)} - \alpha^{(u)} e_q^-(\vec{j}^b)$$

for MULI, and substituting  $f_q^{\text{p.c.}(u)}$ , one gets the normal momentum values  $\sum_{q=1}^{Q-1} f_q(t+1)c_{qn}$  as:

$$\begin{aligned} \text{MULI, MYLI: } j_n(t+1) &= j_n^b(\hat{t}), \\ \text{MCLI, MR1: } \frac{1}{2}(j_n(t+1) + j_n(t)) &= j_n^b(\hat{t}). \end{aligned} \quad (5.35)$$

Computing the anti-symmetric component in a given boundary node,

$$n_q^-(t+1) = \frac{f_q(t+1) - f_{\bar{q}}(t+1)}{2} - e_q^-(t+1),$$

one gets for  $m_q = \lambda_o n_q^-$ :

$$\begin{aligned} \text{MULI, MYLI: } m_q(\vec{r}_b, t+1) &= m_q(\vec{r}_b, t) - \lambda_o(e_q^-(\vec{r}_b, t+1) - e_q^-(\vec{j}^b(\hat{t}))), \\ \text{MCLI, MR1: } m_q(\vec{r}_b, t+1) &= m_q(\vec{r}_b, t) - \lambda_o(e_q^-(\vec{r}_b, t+1) + e_q^-(\vec{r}_b, t) - 2e_q^-(\vec{j}^b(\hat{t}))). \end{aligned} \quad (5.36)$$

Substituting here the solution (5.35),  $m_q(t)$  becomes fixed for the *populations perpendicular to the boundary*:

$$\text{MLI}(\alpha^{(u)}, \text{MR1: } m_q(\vec{r}_b, t+1) = m_q(\vec{r}_b, t), \quad |c_{qn}| = 1, \quad |c_{q\tau}| = 0. \quad (5.37)$$

Numerical simulations with the parabolic schemes in open and closed rectangular boxes, taking  $\delta_q = 0$  for the vertical and/or horizontal boundaries, confirm that  $m_q(t) \equiv m_q(0)$  for the normal populations. Exact *steady* closure relation (5.11) becomes for all cut links when  $\delta_q = 0$ :

$$\text{MGLI}(\alpha^{(u)}, \text{CLI: } (j_q^* + \beta^{(f^*)}(F_q^* - m_q^{(F)}))(\vec{r}_b) = j_q^*(\vec{r}_w), \quad \vec{r}_b = \vec{r}_w, \quad (5.38)$$

$$\text{MLI}(\alpha^{(u)}, \text{MR1: } j_q^*(\vec{r}_b) = j_q^*(\vec{r}_w), \quad \vec{r}_b = \vec{r}_w. \quad (5.39)$$

The conditions imposed by relation (5.38) constrain not only  $j_q^*$  but also  $m_q$ . This constraint is not exact unless  $\beta^{(p^*)}m_q^{(F)} + \beta^{(f^*)}F_q^* + f_q^{\text{p.c.}(u)}$  vanishes, e.g. for Couette flow. In contrast, the closure relation (5.39) is exact but it does not restrict the non-equilibrium components. The obtained steady velocity solution is then *exact* at *boundary points* for

any solution obtained in the bulk. The population solution depends however on the initial values  $m_{q\perp}(\vec{r}_b, 0)$  assigned for the normal links  $q\perp$ . For some (invariant) situations discussed in [22] the associated accommodation layer has not any impact on the velocity solution. In general, however, it is not so and the velocity solution loses the uniqueness, depending on the initialization of  $m_{q\perp}(\vec{r}_b, 0)$ .

We recommend to avoid the use of the parabolic schemes (based currently on the explicit in time  $f_q^{\text{p.c.}(u)}$  corrections) when  $\delta_q = 0$ . Finally, we emphasize that the situation  $\delta_q = 0$  can be avoided by replacing the grid solid vertex by the next neighbor node, then  $\delta_q = 0$  is replaced by  $\delta_q = 1$ , but this may increase the truncation errors.

## 5.6 Time approximation

The third-order accurate closure relation (5.3) is:

$$\begin{aligned} \text{MLI}(\alpha^{(u)}), \text{MR}(k): (j_q^* + \delta_q \partial_q j_q^* + \frac{1}{2} \delta_q^2 \partial_q^2 j_q^* + \alpha^{(t)} \partial_t j_q^*)(\vec{r}_b, t) &= j_q^*(\vec{r}_w, \hat{t}) \\ \text{LI}(\alpha^{(u)}): (\alpha^{(u)} (j_q^* + \delta_q \partial_q j_q^* + \beta^{(p^*)} m_q^{(F)} + \beta^{(f^*)} F_q^* + \alpha^{(t)} \partial_t j_q^*) + f_q^{\text{p.c.}(u)})(\vec{r}_b, t) & \quad (5.40) \\ &= \alpha^{(u)} j_q^*(\vec{r}_w, \hat{t}). \end{aligned}$$

We conjecture that for time dependent boundary values,  $\alpha^{(t)}$  indicates at what time value  $\hat{t} = t + \alpha^{(t)}$  it is better to set  $w_q^{(u)}(\vec{r}_w, \hat{t})$ .

When  $f_q^{\text{p.c.}(u)} = 0$  then

$$\alpha^{(t)} = \frac{D^- + 1}{\alpha^{(u)}} = \frac{1}{2} - \Lambda_o$$

(see  $\alpha^{(t)}$  in Table 2 with relations (4.8) for  $D^-$ ). It is noted that  $D^-$  is the coefficient of  $m_q$  (since  $m_q$  contains  $\partial_t j_q^*$  via relations (2.22)) and  $+1$  comes from the change of the momentum in time:

$$(\alpha^{(u)} - 1) j_q^*(\vec{r}_b, t) + j_q^*(\vec{r}_b, t+1) = \alpha^{(u)} j_q^*(\vec{r}_b, t) + \partial_t j_q^*.$$

Then, if  $f_q^{\text{p.c.}(u)}$  includes  $\beta \alpha^{(u)} m_q^{(F)}$  (for some  $\beta$ ),  $\alpha^{(t)}$  is increased with  $\beta$  and becomes equal to  $\frac{1}{2} - \Lambda_o + \beta$ . When the second-order spatial error is canceled, as for the  $\text{MLI}(\alpha^{(u)})$  and  $\text{MR}(k)$  families, we suggest that this expression presents an effective estimate of  $\alpha^{(t)}$ , e.g.  $\beta = \Lambda_o$  for  $\text{MR}(k)$  and  $\beta = \Lambda_o + |\delta_q - \frac{1}{2}|$  for  $\text{MULI}/\text{MDLI}$ . The resulting coefficient  $\alpha^{(t)}$  is presented in Table 8. For the principal parabolic schemes,  $\alpha^{(t)}$  is found between  $\frac{1}{2}$  and 1.

The second-order space and times errors are difficult to separate for the  $\text{LI}(\alpha^{(u)})$  family. The formal estimate for  $\alpha^{(t)}$  is  $\frac{1}{2} - \Lambda_o + \beta$ , with  $\beta$  again as the  $m_q^{(F)}$  coefficient in  $f_q^{\text{p.c.}(u)}$ . However, when the component  $-\Lambda_o (\partial_t j_q^* + \partial_q \Pi_q^* - F_q^*)$  of the second-order error is expressed via  $\Lambda_e \partial_q^2 j_q^*$ , as in the special solution (5.12) for  $\Lambda_{e0}(\delta_q)$ , it contributes to space error and we suggest that the *effective* coefficient reduces then to  $\frac{1}{2} + \beta$ . We summarize this in Table 8.

Table 8: Coefficient  $\alpha^{(t)}$  in closure relation (5.3). When the second-order time and space errors are coupled for the linear schemes, e.g., via the effective solutions for  $\Lambda_{eo}$ , the solutions of the parabolic schemes (second line) are valid for linear schemes and replace the fourth line.

$M_q^{(u)}$	MULI	MDLI	MYLI	MCLI, MR( $k$ )
$\alpha^{(t)}$	$1 - \delta_q$	$\delta_q$	1	$\frac{1}{2}$
$M_q^{(u)}$	MGULI	MGDLI	MGYLI	CLI, BB
$\alpha^{(t)}$	$1 - \delta_q - \Lambda_o$	$\delta_q - \Lambda_o$	$1 - \Lambda_o$	$\frac{1}{2} - \Lambda_o$

We verify this analysis in [22] modeling time-harmonic flow [26,47] with time dependent boundary conditions at the inlet/outlet sections. This and other tests (e.g., transient Couette flow and Taylor vortex flow) mainly indicate that MR1 behaves more accurately when the boundary values are estimated in the middle of the time interval,  $\hat{t} = t + \frac{1}{2}$ ; CLI and MCLI have a better accuracy with  $\hat{t} = t + \frac{1}{2}$  but only when  $\delta_q \leq \frac{1}{2}$ , then the results are close for  $\alpha^{(t)} = \frac{1}{2}$  and  $\alpha^{(t)} = 1$ , and  $\hat{t} = t + 1$  gets better results when  $\delta_q \rightarrow 1$ . The MYLI and MGYLI behave more accurately with  $\hat{t} = t + 1$  for all  $\delta_q$ .

## 6 $M_q^{(p)}$ -schemes for pressure boundary condition

We assume that the pressure distribution and the tangential velocities are prescribed at the boundary  $\Gamma^{(p)}$ :

$$P|_{\Gamma^{(p)}} = P^b(\vec{r}_w, t), \quad \vec{u}_\tau|_{\Gamma^{(p)}} = u_\tau^b(\vec{r}_w, t), \quad \vec{r}_w \in \Gamma^{(p)}, \quad \tau = \{\tau_1, \tau_2\}. \tag{6.1}$$

The multi-reflection combination  $M_q$  is called  $M_q^{(p)}$  for the Dirichlet pressure condition. The  $M_q^{(p)}$ -scheme follows relations (4.2) with:

$$\begin{aligned} f_{\bar{q}}(\vec{r}_b, t+1) &= M_q^{(p)}(\vec{r}_b, t), \\ M_q^{(p)} &= R_q^{(p)}(\vec{r}_b, t) + f_q^{\text{p.c.}(p)}(\vec{r}_b, t) + w_q^{(p)}(\vec{r}_w, \hat{t}), \quad q \in \Pi^{(p)}, \\ w_q^{(p)} &= -\alpha^{(p)} e_q^+(\vec{r}_w, \hat{t}) = -\alpha^{(p)} \Pi_q^*(c_s^{-2} P^b, \vec{j}^b, \rho_0), \\ f_q^{\text{p.c.}(p)} &= -\beta^{(u)} p_q(\vec{r}_b, t). \end{aligned} \tag{6.2}$$

Table 9 summarizes the principal  $M_q^{(p)}$  schemes developed in this paper: (*pressure anti-bounce-back*) PAB, (*pressure linear interpolation*) PLI and the five-populations based PMR( $k$ ) family, where  $k$  is a free parameter. Table 10 presents the closure conditions of the  $M_q^{(p)}$

Table 9: The coefficients  $\kappa_1, \kappa_0, \kappa_{-1}, \bar{\kappa}_{-1}, \bar{\kappa}_{-2}$  for the  $M_q^{(p)}$ -schemes.

$M_q^{(p)}$	PAB	PLI	PMR( $k$ )
$\kappa_1$	-1	$\frac{1}{2} - \delta_q$	$1 + \lambda_e$
$\kappa_0$	0	$\delta_q - 1$	$-1 + \frac{3\lambda_e(k-2) + \delta_q k(2+3\lambda_e)}{4}$
$\kappa_{-1}$	0	0	$-\frac{k\delta_q}{2} - \lambda_e \frac{k-2+3\delta_q k}{4}$
$\bar{\kappa}_{-1}$	0	$\frac{1}{2}$	$1 + \frac{\delta_q k(\lambda_e - 2) + \lambda_e(3k-2)}{4}$
$\bar{\kappa}_{-2}$	0	0	$\frac{-k\delta_q(\lambda_e - 2) - \lambda_e(k-2)}{4}$
$\delta_q$	$\frac{1}{2}$	$0 \leq \delta_q \leq 1$	$0 \leq \delta_q \leq 1$

schemes. We fit it to the link-wise Taylor expansion for  $\Pi_q^*$ :

$$\begin{aligned}
 \alpha^{(p)}(\Pi_q^* + \delta_q \partial_q \Pi_q^* + \frac{1}{2} \delta_q^2 \partial_q^2 \Pi_q^* + \alpha^{(t)} \partial_t \Pi_q^*)(\vec{r}_b, t) &= \alpha^{(p)} \Pi_q^*(\vec{r}_w, \hat{t}) + Err^{(p)}, \\
 Err^{(p)} &= Err_1^{(p)} + Err_2^{(p)} + Err_3^{(p)}, \quad Err_1^{(p)} = (\alpha^{(p)} \delta_q - \beta^{(p)}) \partial_q \Pi_q^*, \\
 Err_2^{(p)} &= -\gamma^{(u)} \partial_q^2 j_q^*, \quad Err_3^{(p)} = -(\gamma^{(p)} + \beta^{(u)} \Lambda_o - \frac{\alpha^{(p)}}{2} \delta_q^2) \partial_q^2 \Pi_q^*, \\
 \alpha^{(t)} &= -\frac{1+B^-}{\alpha^{(p)}}.
 \end{aligned}
 \tag{6.3}$$

All schemes yield  $\alpha^{(u)} = 0$  (i.e.,  $D^- = -1, \beta^{(f)} = 0$ ) such that the terms associated with  $j_q, \partial_t j_q$  and the forcing vanish from the closure relation (see in Table 2). All schemes yield

$$\beta^{(p)} = \alpha^{(p)} \delta_q, \quad 0 \leq \delta_q \leq 1,$$

then  $Err_1^{(p)}$  vanishes (with  $\delta_q = \frac{1}{2}$  for PAB). The first gradient  $\beta^{(u)} \partial_q j_q^*$  is removed with the help of the correction  $f_q^{p.c.(p)}$  (see (6.2)). Since  $p_q(j_q^*)$  includes  $\Lambda_o \partial_q F_q^*$ , the force gradient term  $\gamma^{(f)} \partial_q F_q^*, \gamma^{(f)} = \beta^{(u)} \Lambda_o$ , also vanishes from the closure relation (see relations (4.9)).

The  $M_q^{(u)}$  needs  $\rho(\vec{r}_w)$  to compute  $w_q^{(u)}(\vec{r}_w, \hat{t})$  and, unless  $g_S = 0$ , the  $M_q^{(p)}$  needs the boundary velocity values,  $\vec{u}(\vec{r}_w, \hat{t})$ , to compute the non-linear term in  $w_q^{(p)}(\vec{r}_w, \hat{t})$ , unless  $g_S = 0$ . The simplest directional f.d. approximation can be used:

$$\begin{aligned}
 \vec{u}(\vec{r}_w, \hat{t}) &\approx \vec{u}(\vec{r}_b, t) + \delta_q (\vec{u}(\vec{r}_b, t) - \vec{u}(\vec{r}_b - \vec{c}_q, t)), \quad \text{if } \vec{c}_q \notin \Pi^{(u)}(\vec{r}_b), \\
 \vec{u}(\vec{r}_w, \hat{t}) &\approx \vec{u}(\vec{r}_b, t) + \frac{\delta_q}{\delta_{\bar{q}}} (\vec{u}(\vec{r}_b, t) - \vec{u}(\vec{r}_w, t)), \quad \text{if } \vec{c}_{\bar{q}} \in \Pi^{(u)}(\vec{r}_b), \delta_{\bar{q}} \neq 0.
 \end{aligned}
 \tag{6.4}$$

The last relation applies for the second-type link when  $\vec{r}_w \in \Gamma^{(p)}, \vec{r}_w \in \Gamma^{(u)}$  and  $\delta_{\bar{q}} \neq 0$ . Otherwise, when  $\delta_{\bar{q}} = 0$ , then  $\vec{r}_w$  lies on  $\Gamma^{(u)}$  and one can compute the f.d approximation

Table 10: Coefficients of the pressure closure relations with the  $f_q^{p.c.(p)}$  correction (6.2). The LHS is a linear combination of the elements in the first line. The RHS is equal to  $-w_q^{(p)}/\alpha^{(p)} = \Pi_q(\vec{r}_w, \hat{t})$ . PAB:  $\alpha^{(p)} = -2$ , PLI:  $\alpha^{(p)} = -1$ , PMR( $k$ ):  $\alpha^{(p)} = k\lambda_e$ .

LHS	$\Pi_q^*$	$\partial_q \Pi_q^*$	$\partial_q^2 \Pi_q^*$	$\partial_q^2 j_q^*$	$\partial_t \Pi_q^*$
$M_q^{(p)}$	$\alpha^{(p)}/\alpha^{(p)}$	$\beta^{(p)}/\alpha^{(p)}$	$(\gamma^{(p)} + \beta^{(u)} \Lambda_o)/\alpha^{(p)}$	$\gamma^{(u)}/\alpha^{(p)}$	$\alpha^{(t)}/\alpha^{(p)}$
PAB	1	$\frac{1}{2}$	0	$-\frac{1}{2}\Lambda_e$	$\frac{1}{2}$
PLI	1	$\delta_q$	0	$-\delta_q \Lambda_e$	$2 - \delta_q$
PMR( $k$ )	1	$\delta_q$	$-(\frac{1}{2} + \delta_q) + \frac{1}{k}$	0	$\frac{1}{2} + \Lambda_e(\frac{2}{k} + \delta_q)$
PMR1 ( $k=1$ )	1	$\delta_q$	$\frac{1}{2} - \delta_q$	0	$\frac{1}{2} + \Lambda_e(2 + \delta_q)$
PMR2 ( $k = \frac{2}{(1+\delta_q)^2}$ )	1	$\delta_q$	$\frac{1}{2}\delta_q^2$	0	$\frac{1}{2} + \Lambda_e((1 + \delta_q)^2 + \delta_q)$

along the coordinate axis,

$$\partial_q \vec{u} = \sum_{\alpha=1}^d \partial_\alpha \vec{u} c_{q\alpha},$$

similar to relations (5.26). Linear velocity approximations, which we use for the non-linear term only, are formally consistent with the  $\mathcal{O}(\epsilon^3)$  overall accuracy. When the tangential velocity  $u_\tau$  is prescribed, one must only approximate the normal velocity component,  $u_n(\vec{r}_w, \hat{t})$ .

### 6.1 Five populations based, PMR( $k$ )-family

This family sets  $\gamma^{(u)} = 0$  ( $Err_2^{(p)} = 0$ ) with the help of its coefficients, keeping  $\kappa_{-1}$  and  $\alpha^{(p)}$  as two free parameters. The range of the coefficients improves if one sets:  $\alpha^{(p)} = k\lambda_e$  and specifies  $\kappa_{-1}$  as a linear function of  $\lambda_e$  (see in Appendix B). The coefficients  $\kappa_1 - \bar{\kappa}_{-2}$  are found inside the heuristic stability interval  $[-1, 1]$  when  $\frac{2}{3} \leq k \leq \frac{6}{5}$  and  $k$  is independent of  $\delta_q$  and  $\lambda_e$ . The PMR( $k$ ) is considered as a principal pressure family with  $j^{(3)}/\Pi^{(2)}/F^{(2)}$  accuracy, i.e. exact for linear pressure and parabolic velocity distribution. We apply mostly PMR1=PMR( $k=1$ ). The particular choice, PMR2=PMR( $k=2(1+\delta_q)^{-2}$ ) yields a triplet  $j^{(3)}/\Pi^{(3)}/F^{(2)}$ : it cancels  $Err_3^{(p)}$  owing to  $k$  and becomes exact for parabolic pressure and velocity solutions. The PMR2 yields all its coefficients inside  $[-1; 1]$  for all  $\lambda_e$ . The coefficient  $\alpha^{(t)}$  in Table 10 indicates that the pressure boundary value should be prescribed in the middle of the time interval when  $\Lambda_e \rightarrow 0$  (i.e.  $\Lambda_{e0} \rightarrow 0$  and truncation errors vanish). We emphasize that the estimations for  $\alpha^{(t)}$  are only indicative, its actual values, e.g. for compressible flow, will depend on the coupling with the second-order spatial pressure gradients governed by the coefficients  $\gamma^{(p)}$ .

**Parametrization properties.** Again, the local solution components are labeled with “*loc*” and those in  $\vec{r}_b - \vec{c}_q$  with “*nb*”. Then the exact steady closure relation (4.5) with (4.6) becomes for the PMR( $k$ )–family:

$$\begin{aligned} & (A^{(p)}\Pi_q^*)^{loc} + (A^{(p)}\Pi_q^*)^{nb} + (B^{(p)}m_q^{(F)})^{loc} + (B^{(p)}m_q^{(F)})^{nb} \\ & + A^{(u)nb}(j_q^{*nb} - j_q^{*loc}) + B^{(u)nb}(p_q^{nb} - p_q^{loc}) \\ & + A^{(u)nb}\Lambda_o(F_q^{*nb} - F_q^{loc}) = \alpha^{(p)}\Pi_q^{*b}, \end{aligned} \quad (6.5)$$

where

$$\begin{aligned} \frac{A^{(p)loc}}{\lambda_e} &= -1 + k\left(\frac{3}{2} + \delta_q\right), & \frac{A^{(p)nb}}{\lambda_e} &= 1 - k\left(\frac{1}{2} + \delta_q\right), \\ \frac{B^{(p)loc}}{\lambda_e} &= -\frac{3}{4}(k-2) + \delta_q k(\Lambda_{eo} - \frac{1}{2}), & \frac{B^{(p)nb}}{\lambda_e} &= \frac{1}{4}(k-2) - \delta_q k(\Lambda_{eo} - \frac{1}{2}), \\ \frac{A^{(u)nb}}{\lambda_e} &= \delta_q k \Lambda_e, & \frac{B^{(u)nb}}{\lambda_e} &= \left(\frac{k}{2}(1 + \delta_q) - 1\right)\Lambda_e. \end{aligned} \quad (6.6)$$

Multiplying the closure relation (6.5) by  $\Lambda_o/\lambda_e$  and provided that  $k$  is independent of the eigenvalues (or depends on them via  $\Lambda_{eo}$ ), the coefficients satisfy the sufficient conditions (4.7). The PMR( $k$ ) family supports then exactly the parametrization of the steady bulk solutions.

It is noted that for the PMR2 scheme  $k=2$  when  $\delta_q=0$ , then all coefficients (6.6) vanish with the exception  $A^{(p)loc} = \alpha^{(p)}$  and the exact closure relation becomes:

$$\Pi_q^*(\vec{r}_b) \equiv \Pi_q^b(\vec{r}_w), \quad \delta_q=0, \quad \vec{r}_b = \vec{r}_w, \quad q \in \Pi^{(p)}. \quad (6.7)$$

Like the parabolic velocity schemes, PMR2 yields the exact closure condition for  $\delta_q=0$  and may cause a loss of uniqueness, because of the lack of restriction on the non-equilibrium part. We recommend then to use PMR1 when  $\delta_q=0$ .

## 6.2 One-three populations based, PAB and PLI schemes

The coefficients of PAB and PLI are equal, respectively, to those of the anti-bounce-back and three populations based Dirichlet schemes [18] for diffusion equations. The anti-bounce-back is also used to prescribe the pressure at a free interface, e.g., in [34]. The removal of  $\partial_q j_q^*$  with  $f_q^{p.c.(p)}$  distinguishes the PAB and PLI from their diffusion analogs and improves their accuracy. The exact steady closure relation for PAB (with  $\delta_q = \frac{1}{2}$ ) and PLI is:

$$\alpha^{(p)}(\Pi_q^* + \delta_q m_q^{(F)})(\vec{r}_b) = \alpha^{(p)}\Pi_q^{*b}. \quad (6.8)$$

These relations, and therefore the steady solutions, are equivalent for PAB and PLI for  $\delta_q = \frac{1}{2}$ . They satisfy sufficient parametrization conditions (4.7) (multiplying the relation (6.8) by  $\Lambda_o$ ). These schemes do not remove however  $Err_2^{(p)}$  with their coefficients, with the exception of  $\delta_q = 0$  with PLI, where its closure relation reduces to exact condition (6.7). We usually restrict the application of PLI and PAB to second-type links, where  $Err_2^{(p)}$  can be canceled with a help of the approximation (5.26):

$$f_q^{p.c.(p)} \rightarrow f_q^{p.c.(p)} + F_q^{p.c.-}, \quad F_q^{p.c.-} = -\gamma^{(u)} \partial_q^{2f.d} j_q^* \tag{6.9}$$

Since  $\gamma^{(u)} = \Lambda_e$  for PAB and  $\delta_q \Lambda_e$  for PLI (see in Table 10), this correction does not modify the parametrization properties for  $v \vec{j}$  (Stokes) and  $\vec{j}$  (Navier-Stokes). Finally,  $\alpha^{(t)} = \frac{1}{2}$  for PAB. For PLI,  $\alpha^{(t)} \in [2, 1]$  and  $\alpha^{(t)} \rightarrow 1$  when  $\delta_q \rightarrow 1$  (we suggest then to use  $\alpha^{(t)} = 1$ ).

### 6.3 Special links with $M_q^{(p)}$

For the *first-type* links, we again replace  $\tilde{f}_q(\vec{r}_b - 2\vec{c}_q, t + 1)$  with  $f_q(\vec{r}_b - \vec{c}_q, t)$  (see in Section 4.2). For the *second-type links*, we switch five-population schemes to PAB/PLI.

## 7 $M_q^{(m)}$ -schemes for the mixed (pressure/tangential velocity) boundary condition

Let  $\{\vec{n}, \vec{\tau}_1, \vec{\tau}_2\}$  be a local coordinate system built on the normal vector  $\vec{n}$ , perpendicular to the solid wall at  $\vec{r}_w$ , with tangential vectors  $\vec{\tau} = \{\vec{\tau}_1, \vec{\tau}_2\}$ . The mixed scheme is constructed to prescribe the pressure  $P^b = P(\vec{r}_w, t)$  (as a normal condition) and the tangential velocity  $\vec{u}_\tau^b(\vec{r}_w, t)$  (as a tangential condition) at a smooth part  $\Gamma^{(p)}$  of the solid boundary. Mixed condition can be regarded as a particular form of the third kind condition [23]:

$$\begin{aligned} -P + 2\mu \partial_n u_n |_{\Gamma^{(p)}} &= -P^b(\vec{r}_w, t), \quad \vec{r}_w \in \Gamma^{(p)}, \\ \vec{u}_\tau - \beta \nu \partial_n \vec{u}_\tau |_{\Gamma^{(p)}} &= \vec{u}_\tau^b(\vec{r}_w, t), \quad \vec{u}_\tau = \{u_{\tau_1}, u_{\tau_2}\}, \end{aligned} \tag{7.1}$$

when free parameter  $\beta$  is set equal to zero and the viscous stress component  $\mu \partial_n u_n$  is neglected, e.g., when the normal velocity components are nearly invariant along the normal at the inlet/outlet, as in straight long channels. A local node based approach [15] prescribes the stress components for arbitrary shaped free interface. We believe that it can be adapted for third kind boundary conditions. In this paper, we aim only to show how the MR approach can be extended to mixed, pressure/tangential velocity Dirichlet conditions. The main point is that the closure relations of  $M_q^{(u)}$  and  $M_q^{(p)}$  schemes represent the Taylor directional expansion for  $e_q^-(\vec{r}_w)$  and  $e_q^+(\vec{r}_w)$ , respectively. They cannot prescribe both equilibrium components for each link separately. The idea of the  $M_q^{(m)}$

scheme is to equate the total tangential projections to those of  $M_q^{(u)}$  schemes and the total normal projection to one of  $M_q^{(p)}$  scheme.

Let  $\{c_{qn}, c_{q\tau_1}, c_{q\tau_2}\}$  be projections of  $\vec{c}_q$  on the local coordinate vectors. Assuming that both  $M_q^{(p)}(\vec{r}_b)$  and  $M_q^{(u)}(\vec{r}_b)$  are built for all links which cut the solid boundary  $\Gamma^{(p)}$  at  $\vec{r}_b$ , we look for a local set of corrections  $\{\delta f_{\bar{q}}(\vec{r}_b)\}$ :

$$f_{\bar{q}}(\vec{r}_b, t+1) = M_q^{(m)}, \quad M_q^{(m)} = M_q^{(p)} + \delta f_{\bar{q}}, \quad q \in \Pi^{(p)}. \quad (7.2)$$

Let us introduce  $\delta M_q$  as:

$$\delta M_q = M_q^{(u)} - M_q^{(p)}. \quad (7.3)$$

The corrections  $\{\delta f_{\bar{q}}(\vec{r}_b)\}$  must satisfy the following (equivalent) conditions (the summation goes over all  $q \in \Pi^{(p)}$ )

$$\begin{aligned} \sum f_{\bar{q}} c_{qn} &= \sum M_q^{(p)} c_{qn} && \Leftrightarrow \sum \delta f_{\bar{q}} c_{qn} = 0, \\ \sum f_{\bar{q}} c_{q\tau_1}^2 c_{qn} &= \sum M_q^{(p)} c_{q\tau_1}^2 c_{qn} && \Leftrightarrow \sum \delta f_{\bar{q}} c_{q\tau_1}^2 c_{qn} = 0, \\ \sum f_{\bar{q}} c_{q\tau_2}^2 c_{qn} &= \sum M_q^{(p)} c_{q\tau_2}^2 c_{qn} && \Leftrightarrow \sum \delta f_{\bar{q}} c_{q\tau_2}^2 c_{qn} = 0, \\ \sum f_{\bar{q}} c_{q\tau_1} c_{q\tau_2} c_{qn} &= \sum M_q^{(p)} c_{q\tau_1} c_{q\tau_2} c_{qn} && \Leftrightarrow \sum \delta f_{\bar{q}} c_{q\tau_1} c_{q\tau_2} c_{qn} = 0, \\ \sum f_{\bar{q}} c_{q\tau_1} &= \sum M_q^{(u)} c_{q\tau_1} && \Leftrightarrow \sum \delta f_{\bar{q}} c_{q\tau_1} = \sum \delta M_q c_{q\tau_1}, \\ \sum f_{\bar{q}} c_{q\tau_2} &= \sum M_q^{(u)} c_{q\tau_2} && \Leftrightarrow \sum \delta f_{\bar{q}} c_{q\tau_2} = \sum \delta M_q c_{q\tau_2}. \end{aligned} \quad (7.4)$$

The third, fourth and last equations concern the three-dimensional models only. The two last equations restraint the tangential velocity. The other conditions represent the normal (pressure) constraints. Let us elaborate these relations for the simplest case when  $\Gamma^{(p)}$  is parallel to one coordinate axis.

## 7.1 $d2Q9$ velocity set

For the  $d2Q9$  velocity set three equations are retained:

$$\sum_{q \in \Pi^{(p)}} \delta f_{\bar{q}} c_{qn} = 0, \quad \sum_{q \in \Pi^{(p)}} \delta f_{\bar{q}} c_{q\tau_1}^2 c_{qn} = 0, \quad \sum_{q \in \Pi^{(p)}} \delta f_{\bar{q}} c_{q\tau_1} = \sum_{q \in \Pi^{(p)}} \delta M_q c_{q\tau_1}. \quad (7.5)$$

For a standard node with two incoming diagonal populations and one normal, the solution is:

$$d2Q9: \delta f_{\bar{q}} = -\frac{c_{\bar{q}\tau_1}}{2} \sum_{q \in \Pi^{(p)}} \delta M_q c_{q\tau_1}. \quad (7.6)$$

As one could expect, the normal link sets the pressure condition:

$$\delta f_{\bar{q}} = 0, \quad M_q^{(m)} = M_q^{(p)}$$

when  $c_{\bar{q}\tau_1} = 0$ . Replacing  $\delta M_q$  with its definition, the solution, e.g., at inlet, becomes:

$$\begin{aligned} \text{d2Q9: } \quad f_1 &= M_3^{(p)}, \\ f_5 &= \frac{1}{2}(M_6^{(p)} + M_7^{(p)}) - \frac{1}{2}(M_6^{(u)} - M_7^{(u)}), \\ f_8 &= \frac{1}{2}(M_6^{(p)} + M_7^{(p)}) + \frac{1}{2}(M_6^{(u)} - M_7^{(u)}). \end{aligned} \quad (7.7)$$

## 7.2 d3Q15 velocity set

The second and the third relation (7.4) are identical for a non-inclined wall. The solution for the 5 incoming populations in a standard boundary node is:

$$\text{d3Q15: } \delta f_{\bar{q}} = -\frac{c_{\bar{q}\tau_1}}{4} \sum_{q \in \Pi^{(p)}} \delta M_q c_{q\tau_1} - \frac{c_{\bar{q}\tau_2}}{4} \sum_{q \in \Pi^{(p)}} \delta M_q c_{q\tau_2}. \quad (7.8)$$

Again, the normal population ( $c_{q\tau_1} = c_{q\tau_2} = 0$ ) performs a pressure condition,  $\delta f_{\bar{q}} = 0$ .

## 7.3 d3Q19 velocity set

For a non-inclined wall, the linear system (7.4) reduces to two sub-systems: one for  $c_{qn}c_{q\tau_1} \neq 0$  and another one for  $c_{qn}c_{q\tau_2} \neq 0$  (e.g., when the inlet is perpendicular to the  $x$ -axis,  $c_{q\tau_1} = c_{qy}$  and  $c_{q\tau_2} = c_{qz}$ ). The first equation in (7.4) couples the two sub-systems. The solution for each sub-system has a form (7.6):

$$\begin{aligned} \text{d3Q19: } \quad \delta f_{\bar{q}} &= -\frac{c_{\bar{q}\tau_1}}{2} \sum_{q \in \Pi^{(p)}} \delta M_q c_{q\tau_1}, \quad c_{qn}c_{q\tau_1} \neq 0, \\ \delta f_{\bar{q}} &= -\frac{c_{\bar{q}\tau_2}}{2} \sum_{q \in \Pi^{(p)}} \delta M_q c_{q\tau_2}, \quad c_{qn}c_{q\tau_2} \neq 0, \\ \delta f_{\bar{q}} &= 0, \quad c_{qn} \neq 0, \quad c_{q\tau_1} = 0, \quad c_{q\tau_2} = 0. \end{aligned} \quad (7.9)$$

## 7.4 Special links with $M_q^{(m)}$

Computing  $M_q^{(u)}$  and  $M_q^{(p)}$ , one treats the special links along the rules specified for each of these schemes. Their  $M_q^{(m)}$  combination is determined however only when the system (7.4) is of full rank. This condition is naturally fulfilled in any “standard” boundary node where all populations which bisect  $\Gamma^{(p)}$  are put into  $\Pi^{(p)}(\vec{r}_b)$ .

Let us illustrate now the situation in corners for the  $d2Q9$  velocity set (Fig. 2). The population  $f_7(\vec{r}_b)$  goes through the corner and cuts two boundaries, the vertical one  $\Gamma^{(p)}$  and the horizontal one  $\Gamma^{(u)}$ . When  $q = \{3, 6, 7\}$  are put into  $\Pi^{(p)}(\vec{r}_b)$ , the solution (7.7) is

used for  $\{f_1, f_5, f_8\}$  and  $\{f_2, f_6\}$  are defined with  $M_q^{(u)}$ . When  $q=7$  is put into  $\Pi^{(u)}(\vec{r}_b)$ , i.e.,  $f_5 = M_7^{(u)}$ , then  $f_3$  and  $f_6$  perform the pressure condition:

$$f_1 = M_3^{(p)}, \quad \delta f_1 = 0, \quad f_8 = M_6^{(p)}, \quad \delta f_8 = 0.$$

A more complicated combination of two (or more) conditions is possible but is not considered for the sake of simplicity.

## 7.5 Further simplifications

One needs to approximate  $u_q(\vec{r}_w)$  for two terms,  $w_q^{(u)}(\vec{r}_w, \hat{t})$  and  $w_q^{(p)}(\vec{r}_w, \hat{t})$  (the last one when  $g_S = 1$ ). Assuming that the tangential velocity is prescribed, one can approximate the normal velocity component with relations (6.4). Linear interpolations are sufficient here for  $w_q^{(u)}(\vec{r}_w, \hat{t})$ , at least when  $\partial_{\tau n}^2 u_n = \mathcal{O}(\varepsilon^3)$  as typically happens for the straight channel flow at inlet/outlet. Indeed, the contribution from other second derivatives vanish from the resulting closure relations owing to their projection on  $c_{q\tau}$ . In this way, *when the tangential velocity is approximately constant at the inlet/outlet or equal to zero*, the lower order  $M_q^{(u)}$  components (e.g. LI( $\alpha^{(u)}$ ) schemes) are sufficient for the mixed conditions. The parabolic velocity components in mixed schemes gain usually in accuracy for non-channel flows (see in [22]).

## 8 MR schemes with MRT

The boundary schemes are derived and analyzed above in the context of the TRT model. The same solutions can be obtained using the multiple-relaxation-times (MRT) collision operator, taking all the “symmetric” eigenvalues (associated with the even order polynomial basis vectors) equal to  $\lambda_e$  and all the “antisymmetric” eigenvalues equal to  $\lambda_o$ . However, with the help of distinct symmetric eigenvalues one can assign different values to the bulk and kinematic viscosities (for any  $c_s^2$ ) and improve the stability and acoustic properties (see [36, 37]). In particular a high bulk viscosity can be used to damp the acoustic waves generated by a time-dependent pressure field.

Let us denote the kinematic viscosity eigenvalue as  $\lambda_e$ . We suggest, based on the form of the first order expansion for MRT models (see, e.g., [15, 29]), that under the incompressibility assumption all the derived boundary schemes will keep their accuracy. Indeed, a projection on the second and fourth order polynomial basis vectors (which may have eigenvalues distinct from  $\lambda_e$ ) is proportional to  $\nabla \cdot \vec{j}$ . For incompressible flows,  $\nabla \cdot \vec{j} = \mathcal{O}(\varepsilon^3)$ , then

$$n_q^{+(1)} = \frac{p_q}{\lambda_e} + \mathcal{O}(\varepsilon^3)$$

and the subsequent space approximation keeps its TRT form. For transient flows,  $\partial_t \Pi_q^*$  (also projected on the symmetric basis vectors) vanishes from the velocity closure rela-

tions owing to the selection of the coefficients. Let us consider now the antisymmetric solution component in more detail.

Working with the mass/momentum conserving equilibrium (first setup in relations (2.15) and (2.18)), the values assigned to the relaxation parameters of the conserved basis vectors are irrelevant for MRT. We assume therefore

$$\vec{\mathcal{F}} = \vec{F}, \quad S_q^- = t_q^* (\vec{F} \cdot \vec{c}_q)$$

for MRT. For cubic velocity sets, it is natural to prescribe equal antisymmetric eigenvalues, because of the symmetry. The MRT retains then, like TRT, only one anti-symmetric eigenvalue function  $\Lambda_o$ . It follows that if the coefficients of the selected scheme and their  $f_q^{\text{p.c.}}$  correction do not depend of the “symmetric” eigenvalues, one can apply them directly with MRT. This is the case of all the principal velocity schemes developed here. Their explicit corrections are related to  $m_q$ , equal to the sum of *post-collision* projections on the antisymmetric MRT basis vectors (see also in [16]). However, the approximation (5.26) which we suggest for third-order accuracy in corners keeps its form for incompressible flows only.

The principal  $f_q^{\text{p.c.}(p)}$  correction of the pressure schemes in relations (6.2) equals to  $-\beta^{(u)} p_q(\vec{r}_b, t)$ . The coefficient  $\beta^{(u)} = B^- + D^+$  (see relations (4.9)) depends formally on  $\lambda_e$  via  $D^+$ . However, this correction can be computed in its original form, also valid for MRT:

$$f_q^{\text{p.c.}(p)} = -(B^- + (\alpha^{(p)} + 1)) p_q(\vec{r}_b, t) - \alpha^{(p)} n_q^+(\vec{r}_b, t). \quad (8.1)$$

All other coefficients of PAB and PLI are independent of  $\lambda_e$ . It is not the case for the PMR family and we suggest to compute its coefficients with the kinematic viscosity eigenvalue, under the incompressibility assumption. We emphasize that the estimation of the coefficient  $\alpha^{(t)}$  for time dependent pressure conditions will change its form when the symmetric eigenvalues are distinct, but, most likely, the limit for small viscosity values will not be altered.

One should keep in mind that unlike the TRT where the  $\Lambda_{e0}$  combination is unique, the degrees of freedom of the MRT operator are formed with all the possible  $\Lambda_{e0}$  combinations of the symmetric/antisymmetric eigenvalues. In general, all of them may come as higher-order coefficients in the expansion and influence the solution. Although at steady state this contribution is shifted to the second-order, it spoils the exact parametrization via  $\Lambda_{e0}$ . One should fix all “symmetric/antisymmetric” combinations, via “free” symmetric eigenvalues, when  $\lambda_e$  and  $\lambda_o$  vary with the viscosity and their combination  $\Lambda_{e0}$  is fixed. The interplay between the values assigned to distinct magic combinations is not yet fully understood for stability, higher-order accuracy and parametrization.

## 9 Conclusion

We presented the steady state recurrence equations for the TRT evolution operator and derived the parametrization properties of their solutions in the bulk. One of our objec-

tives was to show that there is a proper parametrization of the free “kinetic” collision component which yields equal non-dimensional macroscopic solutions on a fixed grid. This property is not available for the BGK model, where the second-order boundary errors and all higher order bulk errors are related to powers of the kinematic viscosity. Equivalent equilibrium functions enable the TRT model to operate easily with different formulations for external source terms. In this context, an infinite expansion of the population solution is extended for variable mass and force sources.

When the coefficients of the link-wise boundary scheme satisfy some specific but quite natural conditions, steady numerical solutions are parameterized exactly on a fixed grid and depend, in addition to the hydrodynamic non-dimensional numbers, only on the value assigned to the free collision parameter  $\Lambda_{eo}$ . This property conditions the numerical efficiency of the method. Already known and new, velocity and pressure multi-reflection type boundary schemes are analyzed with respect to this property. Bounce-back, CLI from the LI( $\alpha^{(u)}$ ) family, MR1 and the sub-family MGMR(C) from the MR( $k$ ) family are parameterized exactly as the bulk solution owing to a special form of their coefficients. New “parabolic” schemes: the velocity family MLI( $\alpha^{(u)}$ ) and the pressure family PMR( $k$ ), also obey the parametrization conditions. We propose a special local correction which gets the parametrization property for “linear” velocity schemes based on two or three populations. They form the MGLI( $\alpha^{(u)}$ ) sub-family and include MGULI/MGDLI and MGYLI schemes which are based on the coefficients of references [5, 46].

The selection of the multi-reflection schemes among the infinite number of three- or five-population combinations is currently based on the parametrization properties and/or a heuristic stability argument which assumes that the coefficients of the MR schemes stay inside the interval  $[-1, 1]$  (see also [14, 16]). We find that MGULI/MGDLI do not support staggered solutions and are robust. Their “parabolic” counter-parts MDLI/MULI, as well as MCLI and the sub-family MGMR(C), are often more stable than the MR1 scheme, but the latter is in general more accurate. In the future, we hope to deepen our understanding of the relation between the selection of the boundary scheme and the stability/convergence of the whole algorithm.

Once a generic closure relation for a given family of boundary schemes (e.g., linear, parabolic or diffusive) has been chosen, a Taylor expansion, either along a link or the normal to a wall, allows one to express the difference between the actual boundary condition and the prescribed one. This difference can be interpreted along different lines. Since  $\Lambda_{eo}$  is proportional to the square of the kinematic viscosity for the BGK operator, one possibility is to express the difference in terms of powers of the Knudsen number, e.g., in [4, 43, 45], and hope this can be suitable to model rarefied gas flows. As one example, the Taylor-type closure relation [43] for a mixture of bounce-back and specular reflection is fitted to boundary layer analytical solution [7], with the help of specific force weights distribution (assuming a Poiseuille flow). However  $\Lambda_{eo}$  is a free parameter of the TRT/MRT models, making questionable the “kinetic” interpretation of Lattice Boltzmann closure relations. Whatever, we emphasize that the generic closure relation (5.3) allows to match the coefficients of the first and second gradients in boundary layer so-

lutions via the coefficients of the multi-reflections, with or without the help of  $\Lambda_{eo}$ . The developed methodology is not restricted to link-wise boundary schemes and can be easily extended for node based approaches or diffusive type schemes, some examples being found in [9, 12, 14].

The multi-reflection approach guarantees neither local nor global mass conservations. It only tries to minimize the discrepancy with the bulk solution, and mass fluctuations for transient flow, with the help of advanced accuracy for incoming populations. The question of the sufficiency of the effective closure conditions, realized via the microscopic rules, should probably be asked for any kinetic boundary scheme but it is not yet raised in the LB literature, to the best of our knowledge. We have first met the loss of uniqueness of steady solutions in sharp corner geometries for local (node based) exact schemes [14]. For multi-reflections the system may degenerate in closed geometries, e.g., because of the location of flat walls on *grid nodes*. We find that the parabolic schemes enforce then the exact equilibrium boundary values but do not have a sufficient number of the non-equilibrium constraints. Linear schemes may meet this difficulty in grid corners. Third-order accurate pressure and velocity boundary conditions have been extended for corners but there they compromise link-wise implementation for particular links with no neighbors.

Further numerical tests are presented in a separate paper [22]. They validate the presented analysis with respect to the form of the expansion, the parametrization properties and accuracy of the boundary schemes, their extension to corners as well as for an accurate fitting of time dependent boundary conditions.

## A Macroscopic equations via the Chapman-Enskog expansion

Keeping in mind relation (2.7) and enclosing first the source terms into the equilibrium ( $\mathcal{M}=0, \vec{\mathcal{F}}=0$ ), the two times Chapman-Enskog expansion [11, 29]

$$\partial_q = \varepsilon \partial_{q'}, \quad \partial_q^2 = \varepsilon^2 \partial_{q'}^2, \quad \partial_t = \varepsilon \partial_{t_1} + \varepsilon^2 \partial_{t_2}, \quad (\text{A.1})$$

is involved to express the non-equilibrium in terms of the gradients of the equilibrium components:

$$\begin{aligned} f_q(\vec{r} + \vec{c}_q, t+1) - f_q(\vec{r}, t) &= n_q^{+(1)} + n_q^{+(2)} + n_q^{-(1)} + n_q^{-(2)} + \mathcal{O}(\varepsilon^3), \\ p_q^{(1)} &= \varepsilon(\partial_{t_1} e_q^+ + \partial_{q'} e_q^-), \\ m_q^{(1)} &= \varepsilon(\partial_{t_1} e_q^- + \partial_{q'} e_q^+), \\ p_q^{(2)} &= \varepsilon^2 \partial_{t_2} e_q^+ - \varepsilon^2 [\partial_{q'} \Lambda_o \partial_{t_1} e_q^- + \partial_{q'} \Lambda_o \partial_{q'} e_q^+] - \varepsilon^2 [\partial_{t_1} \Lambda_e \partial_{t_1} e_q^+ + \partial_{t_1} \Lambda_e \partial_{q'} e_q^-] \\ &= \varepsilon^2 \partial_{t_2} e_q^+ - \partial_q \Lambda_o m_q^{(1)} - \partial_{t_1} \Lambda_e p_q^{(1)}, \\ m_q^{(2)} &= \varepsilon^2 \partial_{t_2} e_q^- - \varepsilon^2 [\varepsilon \partial_{q'} \Lambda_e \partial_{t_1} e_q^+ + \partial_{q'} \Lambda_e \partial_{q'} e_q^-] - \varepsilon^2 [\partial_{t_1} \Lambda_o \partial_{t_1} e_q^- + \varepsilon \partial_{t_1} \Lambda_o \partial_{q'} e_q^+] \\ &= \varepsilon^2 \partial_{t_2} e_q^- - \partial_q \Lambda_e p_q^{(1)} - \partial_{t_1} \Lambda_o m_q^{(1)}, \\ n_q^{+(k)} &= \frac{p_q^{(k)}}{\lambda_e}, \quad n_q^{-(k)} = \frac{m_q^{(k)}}{\lambda_o}, \quad \forall k=1, 2, \dots \end{aligned} \quad (\text{A.2})$$

The leading order of relations (2.8) with  $\mathcal{M}=0$ ,  $\vec{\mathcal{F}}=0$  are

$$\sum_{q=0}^{Q-1} p_q^{(1)} = M, \quad \sum_{q=1}^{Q-1} m_q^{(1)} \vec{c}_q = \vec{F},$$

then

$$\varepsilon \partial_{t_1} \rho^{\text{eq}} + \nabla \cdot \vec{j}^{\text{eq}} = M + \mathcal{O}(\varepsilon^2), \quad (\text{A.3})$$

$$\varepsilon \partial_{t_1} \vec{j}^{\text{eq}} + \nabla \cdot \mathbf{\Pi} - \vec{F} = \mathcal{O}(\varepsilon^2), \quad \mathbf{\Pi} = \{P_{\alpha\beta}\} = \sum_{q=1}^{Q-1} e_q^+ c_{q\alpha} c_{q\beta}, \quad (\text{A.4})$$

where

$$\rho^{\text{eq}} = \rho^m + \Lambda_e M, \quad \rho^m = \sum_{q=0}^{Q-1} f_q + \frac{M}{2}, \quad \vec{j}^{\text{eq}} = \vec{j} + \Lambda_o \vec{F}, \quad \vec{j} = \sum_{q=1}^{Q-1} f_q \vec{c}_q. \quad (\text{A.5})$$

At second order:

$$\varepsilon^2 \partial_{t_2} \rho^{\text{eq}} = \nabla \cdot \Lambda_o (\varepsilon \partial_{t_1} \vec{j}^{\text{eq}} + \nabla \cdot \mathbf{\Pi}) + \varepsilon \partial_{t_1} \Lambda_e (\varepsilon \partial_{t_1} \rho^{\text{eq}} + \nabla \cdot \vec{j}^{\text{eq}}), \quad (\text{A.6})$$

$$\begin{aligned} \varepsilon^2 \partial_{t_2} \vec{j}^{\text{eq}} = & \nabla \cdot \left( \frac{\Lambda_e}{3} \nabla \vec{j}^{\text{eq}} \right) + \nabla \cdot \left( \frac{2\Lambda_e}{3} \nabla \cdot \vec{j}^{\text{eq}} \right) + \varepsilon \Lambda_e \partial_{t_1} \nabla \cdot \mathbf{\Pi} \\ & + \varepsilon \partial_{t_1} \Lambda_o (\varepsilon \partial_{t_1} \vec{j}^{\text{eq}} + \nabla \cdot \mathbf{\Pi}). \end{aligned} \quad (\text{A.7})$$

Owing to relations (A.4) and (A.5), the *RHS* of Eq. (A.6) is equal to  $\nabla \cdot \Lambda_o \vec{F} + \varepsilon \partial_{t_1} \Lambda_e M$ . Taking the sum of the first- and second-order relations, and writing the obtained equations with respect to the *macroscopic variables*  $\rho^m$  and  $\vec{j}$ , one gets:

$$\partial_t \rho^m + \nabla \cdot \vec{j} = -\varepsilon^2 \partial_{t_2} \Lambda_e M + \mathcal{O}(\varepsilon^3), \quad (\text{A.8})$$

$$\begin{aligned} \partial_t \vec{j} + \nabla \cdot \mathbf{\Pi} - \vec{F} = & \nabla \cdot \left( \frac{\Lambda_e}{3} \nabla \vec{j} \right) + \nabla \cdot \left( \frac{2\Lambda_e}{3} \nabla \cdot \vec{j} \right) + \varepsilon \partial_{t_1} \Lambda_e \nabla \cdot \mathbf{\Pi} \\ & + \text{err}(\vec{F}) - \varepsilon^2 \partial_{t_2} \Lambda_o \vec{F} + \mathcal{O}(\varepsilon^3), \end{aligned}$$

$$\text{err}(\vec{F}) = \nabla \cdot \frac{\Lambda_e}{3} \nabla \Lambda_o \vec{F} + \nabla \cdot \frac{2\Lambda_e}{3} \nabla \cdot \Lambda_o \vec{F}. \quad (\text{A.9})$$

We omit now the terms  $\varepsilon^2 \partial_{t_2} \Lambda_o \vec{F}$  and  $\varepsilon^2 \partial_{t_2} \Lambda_e M$ , assuming that they will be canceled with the help of the next-order terms,

$$\varepsilon^2 \partial_{t_2} \Lambda_o (\varepsilon \partial_{t_1} \vec{j}^{\text{eq}} + \nabla \cdot \mathbf{\Pi}), \quad \varepsilon^2 \partial_{t_2} \Lambda_e (\varepsilon \partial_{t_1} \rho^{\text{eq}} + \nabla \cdot \vec{j}^{\text{eq}}).$$

Substituting the equilibrium distribution (2.14) for the momentum flux tensor  $\mathbf{\Pi}$ , using then the approximation [11] in the form

$$\Lambda_e \varepsilon \partial_{t_1} \nabla \cdot \mathbf{\Pi} \approx \Lambda_e \nabla \varepsilon \partial_{t_1} P \approx c_s^2 \nabla \Lambda_e (M - \nabla \cdot \vec{j}),$$

and replacing  $c_s^2 \nabla(\rho^{\text{eq}} - \Lambda_e M)$  with  $c_s^2 \nabla \rho^m$ , one gets the compressible Navier-Stokes equations with the variable source terms:

$$\begin{aligned} \partial_t \rho^m + \nabla \cdot \vec{j} &= M + \mathcal{O}(\varepsilon^3), \\ \partial_t \vec{j} + g_S \nabla \cdot \left( \frac{\vec{j} \otimes \vec{j}}{\hat{\rho}} \right) &= -\nabla P + \vec{F} + \nabla \cdot (v \nabla \vec{j}) + \nabla (\nabla \cdot v \zeta \vec{j}) \\ &\quad + \text{err}(\vec{F}) + \mathcal{O}(\varepsilon^3) + \mathcal{O}(u^3), \\ P &= c_s^2 \rho^m, \quad v = \frac{\Lambda_e}{3}, \quad v_\zeta = \Lambda_e \left( \frac{2}{3} - c_s^2 \right). \end{aligned} \quad (\text{A.10})$$

Unlike for the MRT, both bulk and kinematic viscosities are defined via one eigenvalue. The sound velocity  $c_s^2$  is restricted then to the interval  $[0, \frac{2}{3}]$ , both viscosities coincide when  $c_s^2 = \frac{1}{3}$ . Further third-order corrections may appear from the neglected term  $\varepsilon \Lambda_e \partial_{t_1} \nabla \cdot E_q^+(\vec{u})$ , giving rise to *even* order corrections in the definition of  $\vec{F}$  (e.g., see Eq. (6) in [24] with  $\tau = -1/\lambda_e$ ). This and others  $\mathcal{O}(u^3)$  order corrections are omitted in the current work.

When using the “diffusive time scaling” (see review in [33]), then  $t = \varepsilon^2 t_2$ , and dropping  $\partial_{t_1}$  the expansion (A.2) becomes:

$$\begin{aligned} p_q^{(1)} &= \partial_q e_q^-, \quad p_q^{(2)} = \partial_t e_q^+ - \partial_q \Lambda_o m_q^{(1)} = \partial_t e_q^+ - \partial_q \Lambda_o \partial_q e_q^+, \\ m_q^{(1)} &= \partial_q e_q^+, \quad m_q^{(2)} = \partial_t e_q^- - \partial_q \Lambda_e p_q^{(1)} = \partial_t e_q^- - \partial_q \Lambda_e \partial_q e_q^-. \end{aligned} \quad (\text{A.11})$$

The macroscopic equations are first given by relations (A.4) to (A.7) where all the  $\partial_{t_1}$  terms are dropped and  $\varepsilon^2 \partial_{t_2}$  is replaced by  $\partial_t$ . The Navier-Stokes equations take then the form (A.9) but the expansion of the next order is needed to match the bulk viscosity (otherwise, one gets  $v_\zeta = \frac{2}{3} \Lambda_e$ ) and the correction due to the mass source:

$$\rho^m = \sum_{q=0}^{Q-1} f_q + \frac{M}{2}.$$

## B Details of the PMR( $k$ ) family

The five coefficients  $\kappa_1$  to  $\bar{\kappa}_{-2}$  in (4.1) are linear function of  $A^\pm$ ,  $B^\pm$  and  $C^-$ :

$$\kappa_1 = A^+ - (\kappa_0 + \bar{\kappa}_{-1} + \kappa_{-1} + \bar{\kappa}_{-2}), \quad A^+ = 1 + \alpha^{(p)}, \quad (\text{B.1})$$

$$\bar{\kappa}_{-2} = \frac{1}{2}(B^- - B^+), \quad (\text{B.2})$$

$$\bar{\kappa}_{-1} = -\frac{1}{2}A^- - \bar{\kappa}_{-2}, \quad (\text{B.3})$$

$$\kappa_0 = -\frac{1}{2}(B^- + B^+) - 2\kappa_{-1}, \quad (\text{B.4})$$

$$2\kappa_{-1} = C^- - \frac{1}{2}(\kappa_0 - \bar{\kappa}_{-2}). \quad (\text{B.5})$$

Assuming that

$$f_q^{\text{p.c.}(p)} = -\beta^{(u)} p_q$$

removes  $\beta^{(u)} \partial_q j_q$  (see relation (6.2)), and keeping  $\kappa_{-1}$  as a free parameter, we solve

$$\alpha^{(u)} = 0, \quad \beta^{(p)} = \alpha^{(p)} \delta_q, \quad \gamma^{(u)} = 0. \quad (\text{B.6})$$

The solution is

$$\begin{aligned} \kappa_1 &= 1 + 2\kappa_{-1} + \frac{\alpha^{(p)} + 3\alpha^{(p)}\delta_q + \frac{2\alpha^{(p)}\delta_q}{\lambda_e}}{2}, \\ \kappa_0 &= -1 - 3\kappa_{-1} - \frac{(\alpha^{(p)}\delta_q)(2+3\lambda_e)}{2\lambda_e}, \\ \bar{\kappa}_{-1} &= 1 - \kappa_{-1} + \frac{\alpha^{(p)}(1 - \frac{\delta_q(2+\lambda_e)}{\lambda_e})}{2}, \\ \bar{\kappa}_{-2} &= \kappa_{-1} + \frac{\alpha^{(p)}\delta_q(2+\lambda_e)}{2\lambda_e}. \end{aligned} \quad (\text{B.7})$$

This solution becomes linear with respect to  $\lambda_e$  if

$$\alpha^{(p)} = k\lambda_e, \quad \kappa_{-1} = c_1 + c_2\lambda_e,$$

where  $k$ ,  $c_1$ , and  $c_2$  do not depend on  $\lambda_e$ :

$$\begin{aligned} \kappa_1 &= 1 + \frac{1}{2}(4c_1 + (4c_2 + k)\lambda_e + k\delta_q(2+3\lambda_e)), \\ \kappa_0 &= -1 + \frac{1}{2}(-6c_1 - 2\delta_q k - 3\lambda_e(2c_2 + k\delta_q)), \\ \bar{\kappa}_{-1} &= 1 + \frac{1}{2}(k(\lambda_e - \delta_q(2+\lambda_e)) - 2(c_1 + c_2\lambda_e)), \\ \bar{\kappa}_{-2} &= c_1 + c_2\lambda_e + \frac{1}{2}k\delta_q(2+\lambda_e), \\ \kappa_{-1} &= c_1 + c_2\lambda_e. \end{aligned} \quad (\text{B.8})$$

When  $\lambda_e \rightarrow 0$ , then

$$\begin{aligned} \kappa_1 &= 1 + 2c_1 + k\delta_q, \quad \kappa_0 = -1 - 3c_1 - k\delta_q, \\ \bar{\kappa}_{-1} &= 1 - k\delta_q - c_1, \quad \bar{\kappa}_{-2} = c_1 + k\delta_q, \quad \kappa_{-1} = c_1. \end{aligned} \quad (\text{B.9})$$

When  $\lambda_e \rightarrow -2$ , then

$$\begin{aligned} \kappa_1 &= 1 + 2c_1 - 4c_2 - k - 2k\delta_q, \\ \kappa_0 &= -1 - 3c_1 + 6c_2 + 2k\delta_q, \\ \bar{\kappa}_{-1} &= 1 - k - (c_1 - 2c_2), \\ \bar{\kappa}_{-2} &= c_1 - 2c_2 = \kappa_{-1}. \end{aligned} \quad (\text{B.10})$$

From (B.9), condition  $\kappa_1 = 1$  implies

$$c_1 = -\frac{k\delta_q}{2}. \tag{B.11}$$

Then the solution (B.9) becomes

$$\{\kappa_1, \kappa_0, \bar{\kappa}_{-1}, \bar{\kappa}_{-2}, \kappa_{-1}\} = \left\{ 1, -1 + \frac{k\delta_q}{2}, 1 - \frac{k\delta_q}{2}, \frac{k\delta_q}{2}, -\frac{k\delta_q}{2} \right\}. \tag{B.12}$$

The coefficients (B.12) are found inside the interval  $[-1, 1]$  when  $0 \leq k \leq 2$ ,  $0 \leq \delta_q \leq 1$ . Substituting relation (B.11) into (B.10), the coefficients become:

$$\begin{aligned} \kappa_1 &= 1 - 4c_2 - k - 3\delta_q k, \\ \kappa_0 &= 1 + 6c_2 + \frac{7\delta_q k}{2}, \\ \bar{\kappa}_{-1} &= 1 + 2c_2 + \frac{k}{2}(\delta_q - 2), \\ \bar{\kappa}_{-2} = \kappa_{-1} &= -2c_2 - \frac{k\delta_q}{2}. \end{aligned} \tag{B.13}$$

From (B.13), the condition  $\kappa_1 = -1$  implies

$$c_2 = \frac{2 - k - 3\delta_q k}{4}. \tag{B.14}$$

Finally, the PMR( $k$ )–family is given by rel. (B.8) with rel. (B.11), (B.14):

$$\begin{aligned} \kappa_1 &= 1 + \lambda_e, \\ \kappa_0 &= -1 + \frac{3\lambda_e(k-2) + \delta_q k(2+3\lambda_e)}{4}, \\ \bar{\kappa}_{-1} &= 1 + \frac{\delta_q k(\lambda_e - 2) + \lambda_e(3k-2)}{4}, \\ \bar{\kappa}_{-2} &= \frac{-k\delta_q(\lambda_e - 2) - \lambda_e(k-2)}{4}, \\ \kappa_{-1} &= -\frac{k\delta_q}{2} - \lambda_e \frac{k-2+3\delta_q k}{4}, \\ w_q &= -\alpha^{(p)} e_q^+, \quad \alpha^{(p)} = A^+ - 1 = k\lambda_e, \\ f_q^{\text{p.c.}(u)} &= -\beta^{(u)} p_q(\vec{r}_b, t). \end{aligned} \tag{B.15}$$

When  $k$  does not depend on  $\lambda_e$  and  $\delta_q$ , then the condition  $\frac{2}{3} \leq k \leq \frac{6}{5}$  keeps all the coefficients inside  $[-1, 1]$  when  $\lambda_e \rightarrow -2$ . When  $k = 1$ ,  $\delta_q = \frac{1}{2}$ , the solution (B.15) becomes

$$\begin{aligned} &\{\kappa_1, \kappa_0, \bar{\kappa}_{-1}, \bar{\kappa}_{-2}, \kappa_{-1}\} \\ &= \left\{ 1 + \lambda_e, -\frac{3}{8}(2 + \lambda_e), \frac{3}{8}(2 + \lambda_e), \frac{1}{8}(2 + \lambda_e), -\frac{1}{8}(2 + \lambda_e) \right\}. \end{aligned} \tag{B.16}$$

When  $\lambda_e \rightarrow -2$ , the coefficients reduce to the (pressure anti-bounce back) PAB scheme.

## C Connections to [16]

The notations used in this paper (on the left-hand side) are related to those used in [16] as follows:

$$\begin{aligned}
 \lambda_o &= -\lambda_2, & \lambda_e &= -\lambda_v, \\
 \alpha^{(u)} &= A_0, & \beta^{(u)} &= A_1, \\
 \alpha^{(p)} &= (A_p - 1), & B^+ &= A'_p, \\
 B^- &= A_j, & C^- &= A'_j, \\
 \frac{\alpha^{(u)}}{2} - 1 &= A_F, & f_q^{p.c.(u)} &= t_q^* F_q^{p.c.}, \\
 \alpha^{(u)} \left(1 + \frac{1}{\lambda_o}\right) - 1 &= A_v, & m_q &= \widehat{f}_q^{(2)}, \\
 A^+ &= A_p, & w_q^{(u)} &= -w_q t_q^*.
 \end{aligned} \tag{C.1}$$

In this paper, the forcing factor in the momentum definition ( $I_f$  in [16]) is set equal to  $-\frac{1}{2}$  (see first relation (2.15)). It is noted that the expansion in the form (2.22) corresponds to relations (27) and (28) in [16] if one replaces  $\partial_t \Pi_q$  by  $-c_s^2 \nabla \cdot \vec{j}$ , in agreement with first order continuity relation, and  $\partial_t j_q + \partial_q P$  with

$$\frac{\Lambda_e}{3} (\Delta j_q + 2\partial_q \nabla \cdot \vec{j}) - \partial_\alpha \frac{j_q j_\alpha}{\rho},$$

using the projection of the momentum conservation on the velocity  $\vec{c}_q$ .

### References

- [1] P. Adler, *Porous Media: Geometry and Transports*, Butterworth/Heinemann, 1992.
- [2] S. Ansumali and I. V. Karlin, Stabilization of the lattice Boltzmann method by the H theorem: A numerical test, *Phys. Rev. E*, 62 (2000), 7999-8003.
- [3] S. Ansumali and I. V. Karlin, Kinetic boundary conditions in the lattice Boltzmann method, *Phys. Rev. E*, 66 (2002), 26311.
- [4] S. Ansumali, I. V. Karlin, S. Arcidiacono, A. Abbas and N. I. Prasianakis, Hydrodynamics beyond Navier-Stokes: Exact solution to the lattice Boltzmann hierarchy, *Phys. Rev. Lett.*, 98 (2007), 124502.
- [5] M. Bouzidi, M. Firdaouss and P. Lallemand, Momentum transfer of a Boltzmann-lattice fluid with boundaries, *Phys. Fluids*, 13 (2001), 3452-3459.
- [6] J. M. Buick and C. A. Greated, Gravity in a lattice Boltzmann model, *Phys. Rev. E*, 61 (2000), 5307-5320.
- [7] C. Cercignani, *Theory and Application of the Boltzmann Equation*, Scottish Academic, New York, 1975.
- [8] S. Chapman, On the law of distribution of velocities, and on the theory of viscosity and thermal conduction, in a non-uniform simple monoatomic gas, *Philos. T. Roy. Soc. A*, 216 (1916), 279.
- [9] R. Cornubert, D. d'Humières and D. Levermore, A Knudsen layer theory for lattice gases, *Physica D*, 47 (1991), 241-259.

- [10] D. Enskog, The kinetic theory of Phenomena in fairly rare gases, Dissertation, Upsala, 1917.
- [11] U. Frisch, D. d'Humières, B. Hasslacher, P. Lallemand, Y. Pomeau and J. P. Rivet, Lattice gas hydrodynamics in two and three dimensions, *Complex Syst.*, 1 (1987), 649-707.
- [12] I. Ginzbourg, Boundary conditions problems in lattice gas methods for single and multiple phases, Ph.D. thesis, University Paris VI, 1994.
- [13] I. Ginzbourg and P. M. Adler, Boundary flow condition analysis for the three-dimensional lattice Boltzmann model, *J. Phys. II France*, 4 (1994), 191-214.
- [14] I. Ginzbourg and D. d'Humières, Local second-order boundary method for lattice Boltzmann models, *J. Stat. Phys.*, 84(5/6) (1996), 927-971.
- [15] I. Ginzburg and K. Steiner, Lattice Boltzmann model for free-surface flow and its application to filling process in casting, *J. Comput. Phys.*, 185 (2003), 61-99.
- [16] I. Ginzburg and D. d'Humières, Multi-reflection boundary conditions for lattice Boltzmann models, *Phys. Rev. E*, 68 (2003), 066614.
- [17] I. Ginzburg, Equilibrium-type and Link-type Lattice Boltzmann models for generic advection and anisotropic-dispersion equation, *Adv. Water Resour.*, 28 (2005), 1171-1195.
- [18] I. Ginzburg, Generic boundary conditions for lattice Boltzmann models and their application to advection and anisotropic-dispersion equations, *Adv. Water Resour.*, 28 (2005), 1196-1216.
- [19] I. Ginzburg, Variably saturated flow described with the anisotropic lattice Boltzmann methods, *J. Comput. Fluids*, 25 (2006), 831-848.
- [20] I. Ginzburg, Lattice Boltzmann modeling with discontinuous collision components. Hydrodynamic and advection-diffusion equations, *J. Stat. Phys.*, 126 (2007), 157-203.
- [21] I. Ginzburg and D. d'Humières, Lattice Boltzmann and analytical modeling of flow processes in anisotropic and heterogeneous stratified aquifers, *Adv. Water Resour.*, 30 (2007), 2202-2234.
- [22] I. Ginzburg, F. Verhaeghe and D. d'Humières, Study of simple hydrodynamic solutions with the two-relaxation-times Lattice Boltzmann scheme, *Commun. Comput. Phys.*, to appear.
- [23] P. M. Gresho, Incompressible fluid dynamics: Some fundamental formulation issues, *Annu. Rev. Fluid Mech.*, 23 (1991), 413-453.
- [24] Z. Guo, C. Zheng and B. Shi, Discrete lattice effects on the forcing term in the lattice Boltzmann method, *Phys. Rev. E*, 65 (2003), 066308.
- [25] H. Hasimoto, On the periodic fundamental solutions of the Stokes equations and their application to viscous flow past a cubic array of spheres, *J. Fluid Mech.*, 5 (1959), 317-328.
- [26] X. He and L.-S. Luo, Lattice Boltzmann model for the incompressible Navier-Stokes equation, *J. Stat. Phys.*, 88 (1997), 927-945.
- [27] F. J. Higuera, S. Succi and R. Benzi, Lattice gas dynamics with enhanced collisions, *Europhys. Lett.*, 9 (1989), 345-349.
- [28] F. J. Higuera and J. Jiménez, Boltzmann approach to lattice gas simulations, *Europhys. Lett.*, 9 (1989), 663-668.
- [29] D. d'Humières, Generalized lattice-Boltzmann equations, in: *AIAA Rarefied Gas Dynamics: Theory and Simulations*, Progress in Astronautics and Aeronautics, vol. 59, 1992, pp. 450-548.
- [30] D. d'Humières, M. Bouzidi and P. Lallemand, Thirteen-velocity three-dimensional lattice Boltzmann model, *Phys. Rev. E*, 63 (2001), 066702.
- [31] D. d'Humières, I. Ginzburg, M. Krafczyk, P. Lallemand and L.-S. Luo, Multiple-relaxation-time lattice Boltzmann models in three dimensions, *Philos. T. Roy. Soc. A*, 360 (2002), 437-451.

- [32] D. d'Humières and I. Ginzburg, Viscosity independent permeability computed with Lattice Boltzmann models: from recurrence equations to "magic" collision numbers, 2007, submitted.
- [33] M. Junk and Z. Yang, Asymptotic analysis of lattice Boltzmann boundary conditions, *J. Stat. Phys.*, 121 (2005), 3-37.
- [34] C. Körner, M. Thies, T. Hoffmann, N. Thürey and U. Rüde, Lattice Boltzmann model for free surface flow for modeling foaming, *J. Stat. Phys.*, 121 (2005), 179-197.
- [35] A. J. C. Ladd, Numerical simulations of particulate suspensions via a discretized Boltzmann equation. Part 2. Numerical results, *J. Fluid Mech.*, 271 (1994), 311-339.
- [36] P. Lallemand and L.-S. Luo, Theory of the lattice Boltzmann method: Dispersion, dissipation, isotropy, Galilean invariance, and stability, *Phys. Rev. E*, 61 (2000), 6546-6562.
- [37] P. Lallemand and L.-S. Luo, Theory of lattice Boltzmann methods: Acoustic and thermal properties in two and three dimensions, *Phys. Rev. E*, 68 (2003), 036706.
- [38] R. Mei, L.-S. Luo, P. Lallemand and D. d'Humières, Consistent initial conditions for lattice Boltzmann simulations, *J. Comput. Fluids*, 35(4) (2006), 855-862.
- [39] D. R. Noble, S. Chen, J. G. Georgiadis and R. O. Buickius, A consistent hydrodynamic boundary condition for the lattice Boltzmann method, *Phys. Fluids*, 7 (1995), 203-209.
- [40] C. Pan, L.-S. Luo and C. T. Miller, An evaluation of lattice Boltzmann schemes for porous media simulation, *J. Comput. Fluids*, 35(4) (2006), 898-909.
- [41] Y. Qian, D. d'Humières and P. Lallemand, Lattice BGK models for Navier-Stokes equation, *Europhys. Lett.*, 17 (1992), 479-484.
- [42] A. S. Sangani and A. Acrivos, Slow flow through a periodic array of spheres, *Int. J. Multiphas. Flow*, 8(4) (1982), 343-360.
- [43] M. Sbragaglia and S. Succi, Analytical calculation of slip flow in lattice Boltzmann models with kinetic boundary conditions, *Phys. Fluids*, 17 (2005), 093602.
- [44] P. A. Skordos, Initial and boundary conditions for the lattice Boltzmann method, *Phys. Rev. E*, 48 (1993), 4823-4842.
- [45] V. Sofonea and R. F. Sekerka, Boundary conditions for the upwind finite difference lattice Boltzmann model: Evidence of slip velocity in micro-channel flow, *J. Comput. Phys.*, 207 (2005), 639-659.
- [46] D. Yu, R. Mei, L.-S. Luo and W. Shyy, Viscous flow computations with the method of lattice Boltzmann equation, *Prog. Aerosp. Sci.*, 39 (2003), 329-367.
- [47] J. R. Womersley, Method for the calculation of velocity, rate of flow and viscous drag in arteries when the pressure gradient is known, *J. Physiol.*, 127 (1955), 553-563.
- [48] G. Zanetti, Hydrodynamics of lattice-gas automata, *Phys. Rev. A*, 40 (1989), 1539-1548.
- [49] Q. Zou and X. He, On pressure and velocity boundary conditions for the lattice Boltzmann BGK model, *Phys. Fluids*, 9 (1997), 1591-1598.